Journal of Asian Earth Sciences 259 (2024) 105911

Contents lists available at ScienceDirect

Journal of Asian Earth Sciences

journal homepage: www.elsevier.com/locate/jseaes

Generation and expulsion of Lower Jurassic hydrocarbon in different source rocks in the Taibei Sag, Turpan-Hami Basin, northwest China

Boran Wang [a,b], Zhilong Huang [a,b,*], Dongsheng Xiao [c], Haiyue Yu [c], Wenren Zeng [a,b], Xin Wang [a,b], Tong Qu [a,b], Zhiyuan Li [a,b], Yizhuo Yang [a,b]

[a] National Key Laboratory of Petroleum Resources and Engineering, China University of Petroleum, Beijing 102249, China
[b] College of Geoscience, China University of Petroleum, Beijing 102249, China
[c] PetroChina Tuha Oilfield Company, Hami 839009, China

ARTICLE INFO

Keywords:
Taibei sag
Sangonghe formation
Lacustrine mudstone
Sedimentary environment
Oil-source correlation
Hydrocarbon generation and expulsion

ABSTRACT

Source rocks in the first (J_1s^1) and second (J_1s^2) members of the Lower Jurassic Sangonghe Formation (J_1s) in the Taibei Sag, Turpan-Hami Basin, NW China, are shore-shallow lacustrine mudstone and semi-deep to deep lacustrine mudstone. These two sets of mudstones provide an excellent opportunity for investigating the origin and expulsion patterns of hydrocarbon from source rocks under different environments. Through systematic geochemical analysis, including total organic carbon (TOC), Rock-Eval analysis, GC-MS analysis, and major and trace element analysis, the geochemical characteristics and sedimentary environment of the Sangonghe Formation (J_1s) source rocks were evaluated. By integrating kerogen kinetics modeling, a more precise assessment of the hydrocarbon generation and expulsion characteristics of the source rocks from both members of the Sangonghe Formation is achieved. The fine-grained sediments of the Sangonghe Formation were formed in a weakly oxidized brackish water body. The J_1s^1 mudstone was deposited in a shore-shallow lacustrine environment. The repeated river influx increased the input of terrestrial higher plants, which complicated the maceral composition and diluted the abundance of organic matter. The J_1s^2 source rocks were formed in the semi-deep to deep lacustrine environment during the maximum transgression period with a large thickness and high TOC values, the maceral composition was dominated by a mixed source of aquatic organisms and terrestrial plants. Consequently, the source rocks of J_1s^2 exhibit higher initial hydrogen index (HI_0), hydrocarbon generation potential (Q_g) and transformation ratio (Tr) compared to those of the J_1s^1 source rocks, while the interbedded mudstone with limited thickness in J_1s^1 exhibits a higher hydrocarbon expulsion efficiency (R_e).

1. Introduction

The fundamental purpose of petroleum exploration is to discover new hydrocarbon-rich reservoirs of commercial value at the lowest cost by using a rapid, efficient approach (Leila et al., 2022; Prinzhofer and Battani, 2003; Tissot and Welte, 1984; Wang et al., 2022a,b). A comprehensive system was established to study the source rock, which is the major factor controlling oil and gas accumulation (Peters and Cassa, 1994; Wu et al., 2022). Further research on hydrocarbon generation and expulsion is necessary to improve the understanding of the potential of source rocks and locate high-quality petroleum reservoirs (Kuhn et al., 2012; Pang et al., 2023).

Total organic carbon (TOC), thermal maturity, and organic matter type significantly influence hydrocarbon generation and expulsion of source rocks (Tissot and Welte, 1984; Chen and Jiang, 2015). The environment in which Chinese shale forms differs significantly from that of marine shales in North American basins; notably, the sedimentary environment of the latter is more stable, rendering the study of the former considerably more challenging (Stoakes, 1980; Stoakes and Creaney, 1984; Wu et al., 2022). In addition, terrestrial lacustrine basins in northwestern China, experienced various changes in the sedimentary environment during the Jurassic period, resulting in the formation of source rock with a more complex kerogen composition (Li et al., 2020c). Therefore, studying the hydrocarbon generation and expulsion characteristics of source rocks formed in different sedimentary backgrounds is a meaningful endeavor.

The lower Jurassic Sangonghe Formation (J_1s) in the Taibei Sag of the Turpan-Hami Basin has become a new field of tight oil reservoir

* Corresponding author at: National Key Laboratory of Petroleum Resources and Engineering, China University of Petroleum, Beijing 102249, China.
E-mail address: huangzhilong1962@163.com (Z. Huang).

https://doi.org/10.1016/j.jseaes.2023.105911
Received 13 April 2023; Received in revised form 28 October 2023; Accepted 1 November 2023
Available online 3 November 2023
1367-9120/© 2023 Elsevier Ltd. All rights reserved.

exploration (He et al., 2022). Insufficient in-depth research on the source rock has substantially hindered the pace of exploration (Dow, 1977; Peters and Cassa, 1994; Jarvie et al., 2007). The Sangonghe Formation developed two sets of source rocks including shore-shallow lacustrine mudstone and semi-deep lacustrine-deep lacustrine mudstone, which provide an excellent example for studying the characteristics of hydrocarbon generation and expulsion of source rocks with different organic matter origins in different sedimentary environment. Because of the special charging conditions of unconventional tight sandstone, the lacustrine mudstone at the top of the Sangonghe Formation has always been regarded as a cap layer. The hydrocarbons in J_1s are believed to be mainly contributed by the lower Badaowan Formation coaly source rock; thus, the hydrocarbon generation potential of the Sangonghe Formation has been neglected (Liu et al., 2012; He et al., 2022).

Regarding hydrocarbon generation and expulsion features, kerogen kinetics experiments and high-temperature pressure thermal simulation experiments are often used to simulate the whole evolution process (Freund et al., 1993), and the generated and expelled hydrocarbons can be quantitatively calculated, accompanied by the analysis of the experimental products (Eseme et al., 2007; Inan et al., 1998; Lafargue et al., 1990; Mann et al., 1997). However, thermal simulation experiments often require high-quality, low-mature source rock samples, and a certain number of samples are required to cover the entire group to increase the reliability of the results and reduce the errors (Chen and Jiang, 2015; Freund et al., 1993). In addition, restoring the temperature and pressure conditions of the in situ subsurface sediments under laboratory conditions is challenging, and the impact of pressure on hydrocarbon generation should also be considered (Chen and Jiang, 2015; Freund et al., 1993). Chen and Jiang (2015) proposed a data-driven model that uses the easily accessible Rock-Eval and TOC datasets to fit an exponential model based on the relationship between the hydrogen index (HI) and T_{max} values. The initial hydrogen index (HI_0) and hydrocarbon transform ratio of source rocks were obtained using the established empirical formula. Li et al., (2020a) improved the model to fix the overestimated initial hydrocarbon index of low-mature source rocks. Scholars have achieved reasonable results by applying the aforementioned model to quantitatively evaluated the hydrocarbon generation and expulsion characteristics of source rocks from their specific research areas based on the theory of material balance and hydrocarbon expulsion threshold (Li et al., 2020a; Pang et al., 2005; Wang et al., 2020; Wu et al., 2022). The advantage of this approach lies in its ease of implementation and efficiency, as well as its ability to incorporate uncertainties arising from sample heterogeneity when managing large amounts of data (Chen and Jiang, 2015; Wang et al., 2020; Wu et al., 2022).

As a new petroliferous field for tight oil and gas exploration in Turpan-Hami Basin, the resource potential of the lacustrine mudstone under the deltaic system of the Lower Jurassic Sangonghe Formation has not been accurately quantified thus greatly hindering the exploration process. This rapid, efficient evaluation method is urgently necessary to evaluate the J_1s source rocks and is a breakthrough in its application to the study area.

The organic and inorganic analysis were applied, using the J_1s in the Taibei Sag (important target strata for unconventional tight oil and gas reservoirs) as an example to: (a) systematically evaluate the quality of source rocks under two distinct sedimentary backgrounds, followed by the determination and comparison of their sedimentary environments and organic matter origins; (b) verify the contribution of the J_1s source rocks to the existing tight sandstone reservoir using detailed oil-source correlation; (c) quantitatively simulate the hydrocarbon generation and expulsion characteristics of source rocks from different sedimentary backgrounds to clarify their differences by applying the newly improved data-driven model. These findings are valuable for objectively assessing the tight oil potential of J_1s source rocks and establishing a theoretical foundation for exploration in Taibei Sag, and provide implications for investigating the kerogen kinetic characteristics of source rock under similar geological conditions in other terrestrial basins with low exploration degrees.

2. Geological background

The Turpan-Hami Basin is located in eastern Xinjiang province (Fig. 1a), bounded by the Bogda structural belt and the Kelami-Mechinola structural belt with an east–west spread of 670 km and a north–south distance of 60–130 km, covering an area of approximately 5.35×10^4 km^2. It has developed a structural pattern consisting of two depressions and one uplift. Three first-level structural belts are developed from west to east: the Turpan Depression, Liaodun Uplift, and Hami Depression (Ni et al., 2019). The Taibei Sag is one of the main secondary tectonic units in the Turpan Depression, adjacent to the Bogda Mountain in the north and bounded by the Huoyanshan-Qiketai structural belt in the south, and can be further divided into Shengbei, Qiudong, and Xiaocaohu Sub-sags (Fig. 1b) (Li et al., 2020c; Liu et al., 2011). The focus areas of this study are Shengbei and Qiudong Sub-sags (Fig. 1c).

The strong compressive tectonic stress during the Jurassic period transformed the early basin pattern and formed a depression-subsidence area near the northern piedmont zone, which made the Turpan-Hami Basin similar to the foreland basin structure (Gong et al., 2016). The Jurassic stratum is the main exploration target in the Taibei Sag, and the source rocks are mainly developed in the Lower Badaowan Formation (J_1b), Sangonghe Formation (J_1s), the Middle Jurassic Xishanyao Formation (J_2x), Qiketai Formation (J_2q) (Fig. 1d), the layer that is focused of this study, can be further divided into two members, J_1s^1 and J_1s^2, from bottom to top (Fig. 1e).

The continental lacustrine-deltaic sedimentary system is developed in J_1s with an upward fining depositional sequence (He et al., 2022). J_1s^1 was deposited in a deltaic system, with frequent fluvial activities and massive sandstone sediments interbedded with inshore-shallow lacustrine dark-grey mudstone. The J_1s^2 sediment was composed of medium-coarse sandstone and pebbly sandstone accompanied by a thick layer of mudstone at the top. This set of mudstone is grey-black semi-deep to deep lacustrine mudstone with a thickness of approximately 30–80 m and is stably distributed, indicating that this set of mudstone was deposited during the period of maximum flooding (Fig. 1e).

3. Data and methods

3.1. Experimental methods

One hundred and twenty-eight source rock samples from drilled cores obtained from 15 wells covering the Shengbei and Qiudong Sub-sags of the Taibei sag were selected for geochemical analyses in this study. Of the samples, 40 and 77 samples were selected from J_1s^1 and J_1s^2 of the Sangonghe Formation, respectively, and 11 samples were selected from the Badaowan Formation for comparison. Fifty samples were selected for gas chromatography-mass spectrometry (GC-MS) analysis, nine of which were extracted oil samples (Table 1). Seventeen samples were selected for major and trace element analyses.

The impurities were removed and all samples were ground into powder (<200 μm) to conduct the geochemical experiments. The TOC content was determined using a Leco CS-230 carbon-surfer analyzer after all inorganic carbon components were removed using dilute hydrochloric acid (Madec and Espitalié, 1985). Rock pyrolysis was tested using a Rock-Eval VI instrument. The pyrolysis products released from kerogen included the free hydrocarbon content (S_1) and cracked hydrocarbon content (S_2), with the maximum pyrolysis peak temperature (T_{max}) recorded during the process. Other key parameters were calculated using the pyrolysis outputs, including hydrogen index ($HI=S_2/TOC\times100$) and generation potential (S_1+S_2) (Tissot and Welte, 1984).

The major and trace elements were determined using an ELEMENT

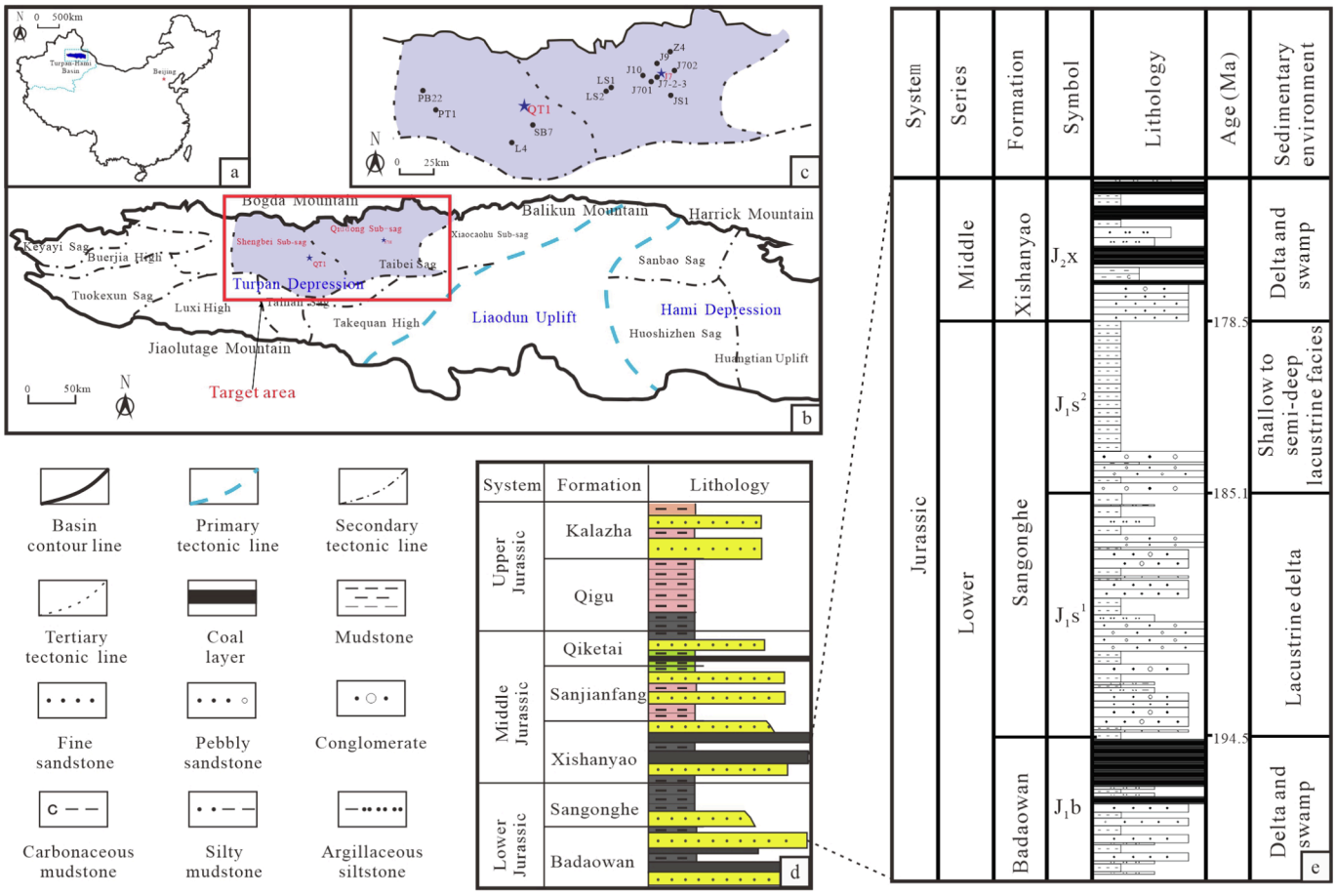

Fig. 1. Geological map of the Taibei Sag. (a) The location of Turpan-Hami Basin. (b) Geologic map of the Turpan-Hami Basin with tectonic units (modified from Li et al., (2020c)). (c). Range of the study area with well locations. (d) Lithological characteristics of the Jurassic strata. (e) The lithology and stratification characteristic of the lower Jurassic strata.

Table 1
Location and numbers of source rock and oil/sand extract samples in the Taibei Sag, Turpan-Hami Basin.

Formation (Fm)		Source rock samples and numbers								oil/sand extract and numbers								
		HQ2	J1	J10	J3	J7H	J701H	J702H	J7-2-3H	P14	PB22	PT1	QT1	J7H	J701H	J702H	J7-2-3H	J10
Sangonghe. Fm (J_1s)	J_1s^2	/	/	2	/	5	2	2	/	/	1	1	3	2	1	3	2	1
	J_1s^1	/	/	/	/	1		2	/	/	/	/	11	/	/	/	/	/
Badaowan. Fm (J_1b)		3	1	/	1	/	/	/	/	3	/	/	3	/	/	/	/	/

XR Plasma Mass Spectrometer. The oxides of major elements were tested using X-ray fluorescence spectrometry (XRF), and the trace elements were tested using inductively coupled plasma mass spectrometry (ICP-MS). The samples were dried, precisely weighted, and dissolved in concentrated nitric and hydrofluoric acid solutions. After dissolution, the residue materials were placed in the acid-driven processor and heated to dry at 160 °C. Five percent diluted nitric acid was added to dissolve the residuals until 50 ml of the solution was available with an analytical precision of better than 0.1 % (Li et al., 2020b; Pan et al., 2020).

The biomarker content in source rock samples was analyzed following the analytical procedure of Moldowan (1984) and Peters and Moldowan (1993). Approximately 100–200 g of each sample powder was extracted with dichloromethane (DCM), and activated copper chips were added to remove the sulfur content within the samples for 24 h by Soxhlet extraction. Saturated hydrocarbons, aromatics, non-hydrocarbons, and asphaltenes were further separated by column chromatography which was filled by 2 g silica gel followed by 3 g alumina. The saturated and aromatic fractions were eluted using petroleum ether and mixed DCM: petroleum ether (2:1, v/v), and the polar fraction was eluted using mixed DCM: methanol (9:1, v/v).

A gas chromatography-mass spectrometry (GC-MS) analysis of saturated hydrocarbon was conducted using an Agilent 5975i mass spectrometer coupled with an Agilent 6890 gas chromatography with a 30 m × 0.25 mm i.d HP-5MS silica capillary column. Helium was used as the carrier gas with a purity of 99.99 % at an average flow rate of 36 cm/s. The initial oven temperature was set to 50 ℃ (hold for 1 min) and then increased to 310 ℃ (hold for 20 min) at the rate of 3 ℃/min. The ionization energy of electron impact was set as 70 eV.

3.2. *A data-driven hydrocarbon generation and expulsion method*

The data used in this study to evaluate the quality of source rock, hydrocarbon generation, and expulsion characteristics were obtained from Rock-Eval pyrolysis and TOC analysis, and the J_1s mudstones were assumed to be homogeneous (Appendix Table 1). The relationship

between HI and T_{max} is simulated to characterize the dynamic properties of hydrocarbon generation during the thermal evolution of kerogen and to restore the initial hydrogen index (HI_0) (Chen and Jiang, 2015; Li et al., 2020a). A sufficient amount of pyrolysis data can ensure that the variation of the T_{max} and HI of samples covers all characteristics of the source rock with a certain type of kerogen during the entire thermal evolution process. Chen and Jiang (2015) established hydrocarbon generation models for different kerogen types, which have been widely used and improved in the latest studies (Feng et al., 2021; Li et al., 2020a; Wang et al., 2020; Wu et al., 2022). Material balance theory was used to determine the hydrocarbon expulsion threshold, recovering the hydrocarbon expulsion process (Pang et al., 2005; Wang et al., 2020). Wang et al. (2020) introduced the mass loss of evaporated hydrocarbon during the expulsion process; thus, a complete hydrocarbon generation and expulsion evaluation process has been determined. The conceptual model is shown in Fig. 2 and the parameters are illustrated in the following section in detail.

This study applied the improved formula proposed by Li et al., (2020a) based on the original version of Chen and Jiang (2015). The new method fixed the problem that the calculated HI is often greater than the original HI due to the existence of constant terms within the immature section (Eq. (1)).

$$HI(Ro) = \frac{HI_o}{1 + \exp\left(\theta \cdot \ln\left(\frac{Ro}{\beta}\right)\right)} \tag{1}$$

where HI_0 is the initial hydrogen index, β and θ are parameters characterizing hydrocarbon generation properties. For a particular type of kerogen, β represents the corresponding Ro when 50 % of organic matter has been converted into hydrocarbons. Meanwhile, θ serves as a parameter that represents the width of the hydrocarbon generation window, illustrating the steepness of the curve slope (Fig. 2). θ is affected by the complexity of the maceral composition and the chemical structure of kerogen. If the maceral composition of kerogen is complex, the θ value tends to be higher, resulting in a wider hydrocarbon generation window. By optimizing these parameters, a trajectory that minimizes the deviation from the measured data is obtained, which was the closest to the change in HI as a function of the thermal evolution of a specific type of kerogen in the practical case.

The hydrocarbon generation potential index Q_g (mg HC /gTOC) is the sum of the remaining hydrocarbon generation index Q_r (mg HC /gTOC) and the hydrocarbon expulsion potential index Q_e (mg HC /gTOC) (Eq. (2)).

$$Q_g = Q_r + Q_e \tag{2}$$

Tr as transformation ratio (%) signifies the fraction of kerogen that has been converted to hydrocarbons in source rocks and can be obtained by Eq. (3) (Chen and Jiang, 2015).

$$T_r = \frac{1200}{HI_0}\frac{(HI_0 - HI)}{(1200 - HI)} \tag{3}$$

Theoretically, Q_g and HI_0 are equal when T_r reaches 100 %, indicating all effective kerogen has been transformed into hydrocarbons. Therefore, Q_g can also be computed using T_r as shown in Eq. (4).

$$Q_g = HI_0 \times T_r \tag{4}$$

When the hydrocarbon generated by the source rock reaches the maximum capacity of kerogen adsorption, the additional hydrocarbon generated will be expelled. This specific thermal maturity level is termed as HET (hydrocarbon expulsion threshold), and the transformation ratio of this point is denoted as T_{re} (%). Q_e (mg HC /gTOC) is calculated using Eq. (5) from Wang et al. (2020), where x denotes the samples with specific values of Ro, and T_{rx} represents the corresponding transform ratio at this point.

$$Q_e = \begin{cases} 0, x < HET \\ \mathrm{HI}_0(T_{rx} - T_{re}), x \geq HET \end{cases} \tag{5}$$

Q_{loss} (mg HC /gTOC) is calculated by Q_r minus Q_m (Eq. (6)), representing the evaporated hydrocarbon potential index as shown in the separated part between Q_m and Q_r curves in Fig. 2.

$$Q_{loss} = Q_r - Q_m \tag{6}$$

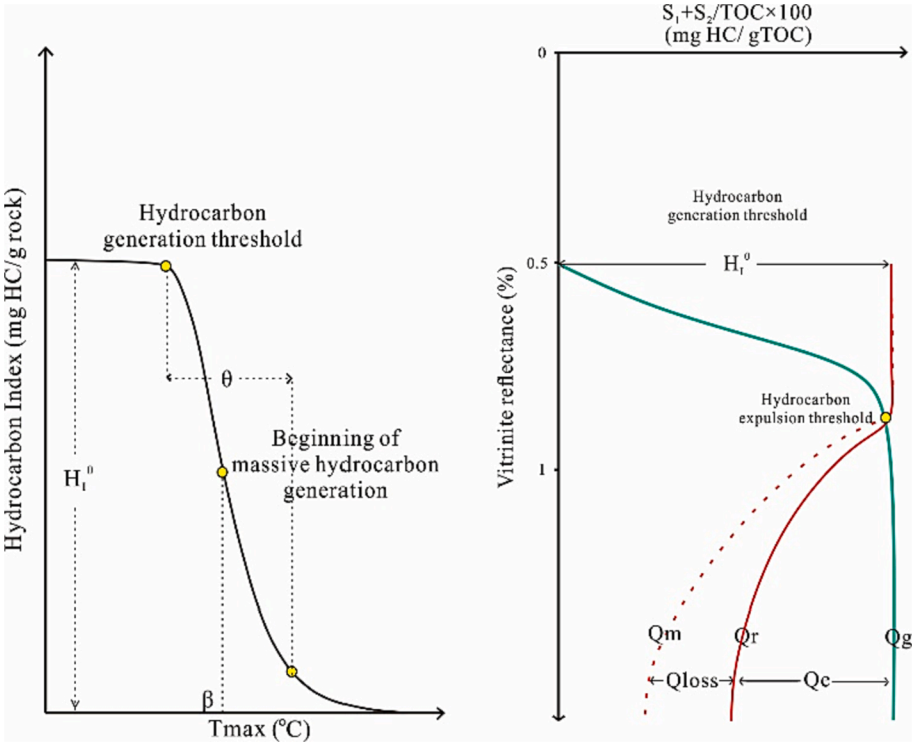

Fig. 2. Conceptual model of the hydrocarbon generation and expulsion (modified from Chen & Jiang, 2015; Li et al., 2020a; Wang et al., 2020).

The ratio of hydrocarbon expulsion to hydrocarbon generation is expressed as the hydrocarbon expulsion efficiency R_e (%) (Eq. (7)). The increased amount of hydrocarbon expulsion per 0.1 % Ro is defined as hydrocarbon expulsion rate V_e (mg HC /gTOC per 0.1 Ro).

$$\mathrm{Re} = \frac{Q_e}{Q_g} \tag{7}$$

$$\mathrm{V_e(Ro)} = \frac{\mathrm{dQ_e}}{\mathrm{dRo}} \tag{8}$$

After the indices of hydrocarbon generation and expulsion were determined, the hydrocarbon generation and expulsion intensities (I_g and I_e, 10^4t/km^2) were calculated using Eq. (9) and Eq. (10) for evaluating the hydrocarbon resource quantity and predicting promising exploration area. Notably, the coefficients in the following equations were modified from those in Wang et al. (2020) to ensure the accuracy of the magnitude.

$$I_g = \int_{Ro^e}^{Ro} Q_g(Ro)*H*\rho*TOC(Ro)*d(Ro)*10^{-1} \tag{9}$$

$$I_e = \int_{Ro^e}^{Ro} Q_e(Ro)*H*\rho*TOC(Ro)*d(Ro)*10^{-1} \tag{10}$$

where H is the source rock thickness (m) and ρ is the source rock density (g/cm^3).

The estimated Ro values were determined from Eq. (11), which was formulated by fitting the correlation between measured Ro and T_{max} of the samples from target formation.

$$\%eRo = 0.0089T_{\max} - 3.0681 \tag{11}$$

4. Results

4.1. Source rocks characteristics

4.1.1. Thickness and distribution

The source rock thickness of J_1s^2 varied from 30 to 80 m and covered most of the Taibei sag (Fig. 3a). For the J_1s^1 source rocks, varying fluvial activities influenced different areas during the deposition period. Mudstone deposits exceeding 70 m in thickness were prominent in the central depression area around QT1 and J7 Wells (Fig. 3b).

4.1.2. Organic matter abundance

The TOC values of J_1s source rocks ranged predominantly between 0.04 % and 10.62 % (avg.1.63 %). The $S_1 + S_2$ values varied between 0.05 and 26.19 (avg. 2.75) mg HC /g Rock. The TOC values of the J_1s^2 source rocks were higher than that of the J_1s^1 samples (Fig. 4). Fig. 5 shows that 79.2 % of the J_1s^2 source rock samples had a TOC higher than 1 % and 11.7 % had a TOC higher than 4.0 %, and more than 54.8 %of the samples from J_1s^1 had a TOC lower than 0.5 %.

The TOC distributions of both members of the Sangonghe Formation exhibited similarities and correlated with the thickness distribution to a certain extent (Fig. 6). The centers of high TOC values were distributed around well QT1 and J7 in the Shengbei and Qiudong Sub-sags,

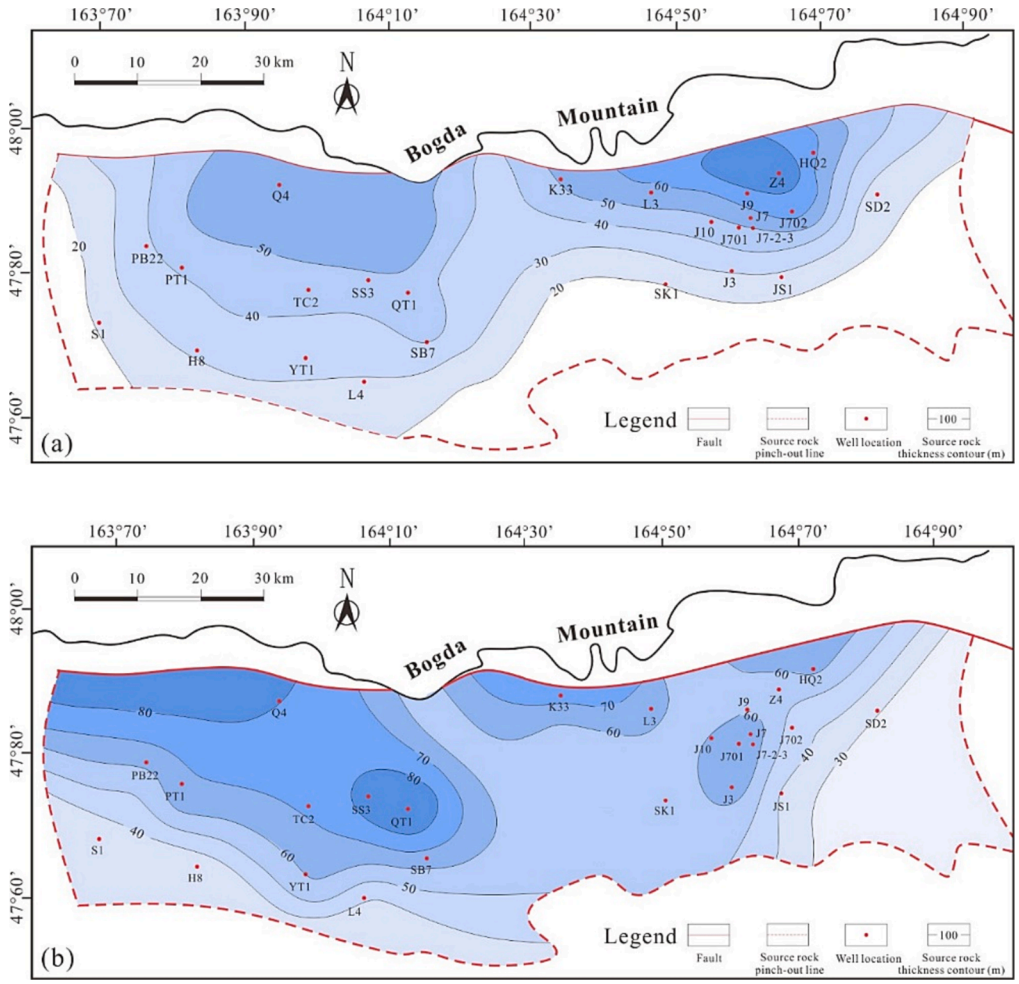

Fig. 3. Thickness contour map of the J_1s^2 source rock (a) and the J_1s^1 source rock (b) of the Sangonghe Formation in the Taibei Sag, Turpan-Hami Basin.

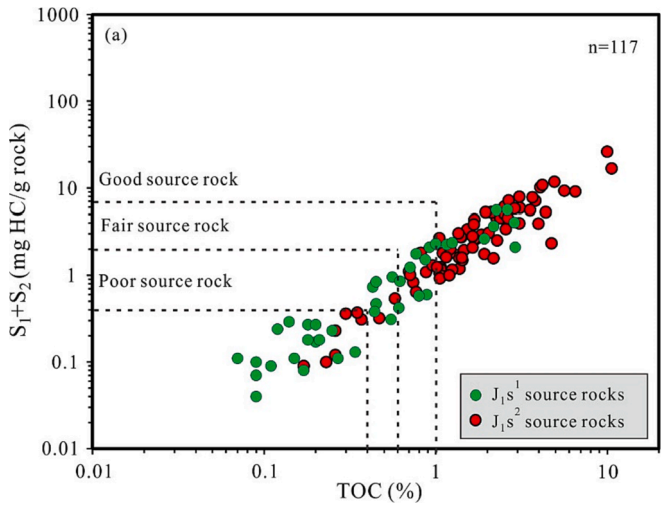

Fig. 4. Plot of (S_1+S_2) vs. Total organic carbon (TOC) of J_1s source rocks (classification criterion according to Peters & Cassa, (1994)).

respectively.

4.1.3. Organic matter type

The kerogen type of J_1s source rock primarily falls into the range of type II_1 and II_2. More than half of the points extend beyond the established boundary, indicating a higher evolution of thermal maturity (Fig. 7). The J_1s^2 samples displayed higher HI values compared to those of J_1s^1. The difference in the variation trends of HI and T_{max} between the J_1s^1 and J_1s^2 samples indicates that the source rocks of these two intervals may have undergone distinct hydrocarbon generation processes.

4.1.4. Thermal maturity

Among the tested samples, the lowest Ro value was 0.94 % and all other test points were greater than 1.0 % with an average of 1.22 % (Fig. 8). The T_{max} distribution histogram showed that most of the samples fell within the range between 440 ℃ and 470 ℃, indicating that the source rocks entered the mature stage, which is the period of hydrocarbon generation. The Ro contour map is based on the measured Ro values of source rock samples obtained from drilled cores and the burial-thermal history reconstruction of uncored wells. Two obvious maturity centers developed around the well QT1 and the J7, both of which were located at the deepest burial depth (Fig. 9). The Ro value of the source rock at the deepest burial depth exceeded 1.2 %, among which the source rock maturity at the location of well QT1 was 0.1 % higher than that of the eastern maturity center because of its larger burial depth.

4.1.5. GC-MS analysis and biomarker parameters

The n-alkanes of the lacustrine source rocks were mainly in the range from C_{13} to C_{35}, displaying unimodal distributions. The n-alkane patterns can be expressed as a single pre-peak with a dominant peak from nC_{16} to nC_{21}, represented by samples from J_1s^2 with their nC_{21-}/nC_{21+} ranging from 0.72 to 4.19 (avg. 3.02), or a single mid-peak or post-peak with the dominant peak from nC_{16} to nC_{26}, represented by samples from J_1s^1 with their nC_{21-}/nC_{21+} ranging from 0.44 to 1.90 (avg. 1.05).

Among the regular steranes, source rock extracts from J_1s^2 showed approximately equal amounts of C_{27} and C_{29} 5α(H), 14α(H), 17α(H)-20R steranes, indicating that it had both aquatic and terrestrial organic matter input. The ααα20RC_{27}/C_{29} ratio of J_1s^2 source rocks ranged from 0.43 to 0.97 (avg. 0.66), higher than that of J_1s^1 (0.23–0.68, avg. 0.45). The isoprenoid alkanes Pr/Ph ratio of the J_1s^2 source rock samples ranged from 1.06 to 3.19 (avg. 1.96), slightly higher than that of the J_1s^1 source rock samples (0.88–1.95, avg. 1.25) (Fig. 10). The gammacerane index (GI = gammacerane/C_{30}H-hopane) of the J_1s^2 source rock samples ranged from 0.16 to 0.43 (avg. 0.27), higher than that of the J_1s^1 (0.10–0.33, avg. 0.23).

4.1.6. Major and trace element analysis

In this study, major and trace element tests were conducted, and the compositions of the relevant elements are listed in Table 2 and Table 3. The Sr concentration in the mudstone samples was lower than that in the upper crust, indicating that lacustrine salinization was relatively low during that period (Pan et al., 2020). SiO_2, Al_2O_3, and Fe_2O_3 are the most abundant oxides, with average values of 58.03 %, 20.54 %, and 5.38 %, respectively. The concentrations of MgO and Na_2O were relatively lower than those in the upper crust, and the contents of other elements were similar to those in the upper crust (Table 3). The calculated Sr/Ba ratio of sediments in J_1s^2 was between 0.16 and 0.29, with an average of 0.24, higher than that of the J_1s^1 sediments (0.12–0.22, avg. 0.16). The Ni/Co ratio of mudstone in J_1s^2 is between 1.41 and 4.51, with an average of 2.39, and the ratio in J_1s^1 is between 1.70 and 2.52, with an average of 2.25. The V/Cr ratio of the J_1s^2 and J_1s^1 source rocks ranges from 0.87 to 2.53 (avg. 1.60) and 1.24–2.37 (avg. 1.86), respectively. The U/Th ratio of J_1s^2 and J_1s^1 source rocks ranges from

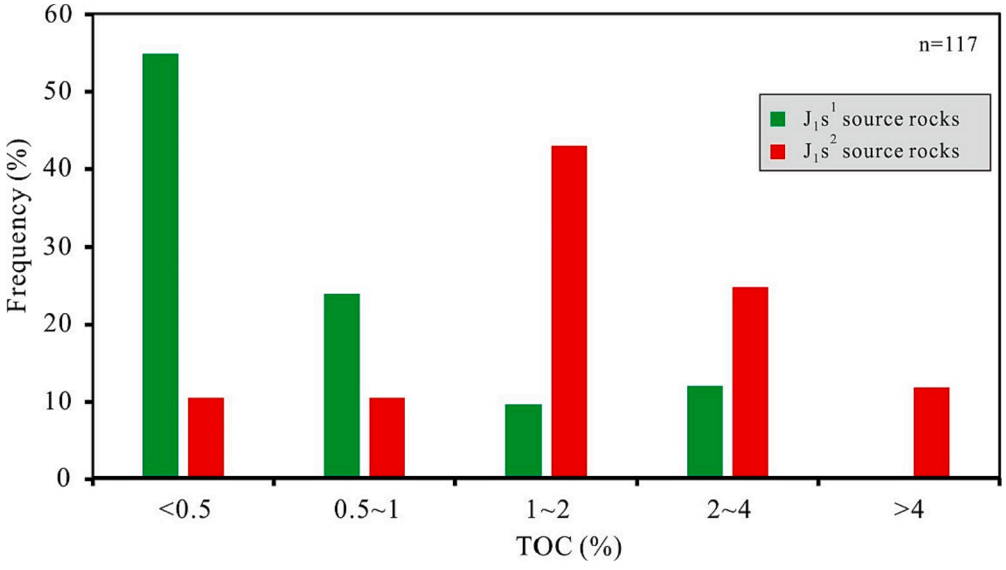

Fig. 5. Histogram of total organic carbon (TOC) of J_1s source rock samples with different quality.

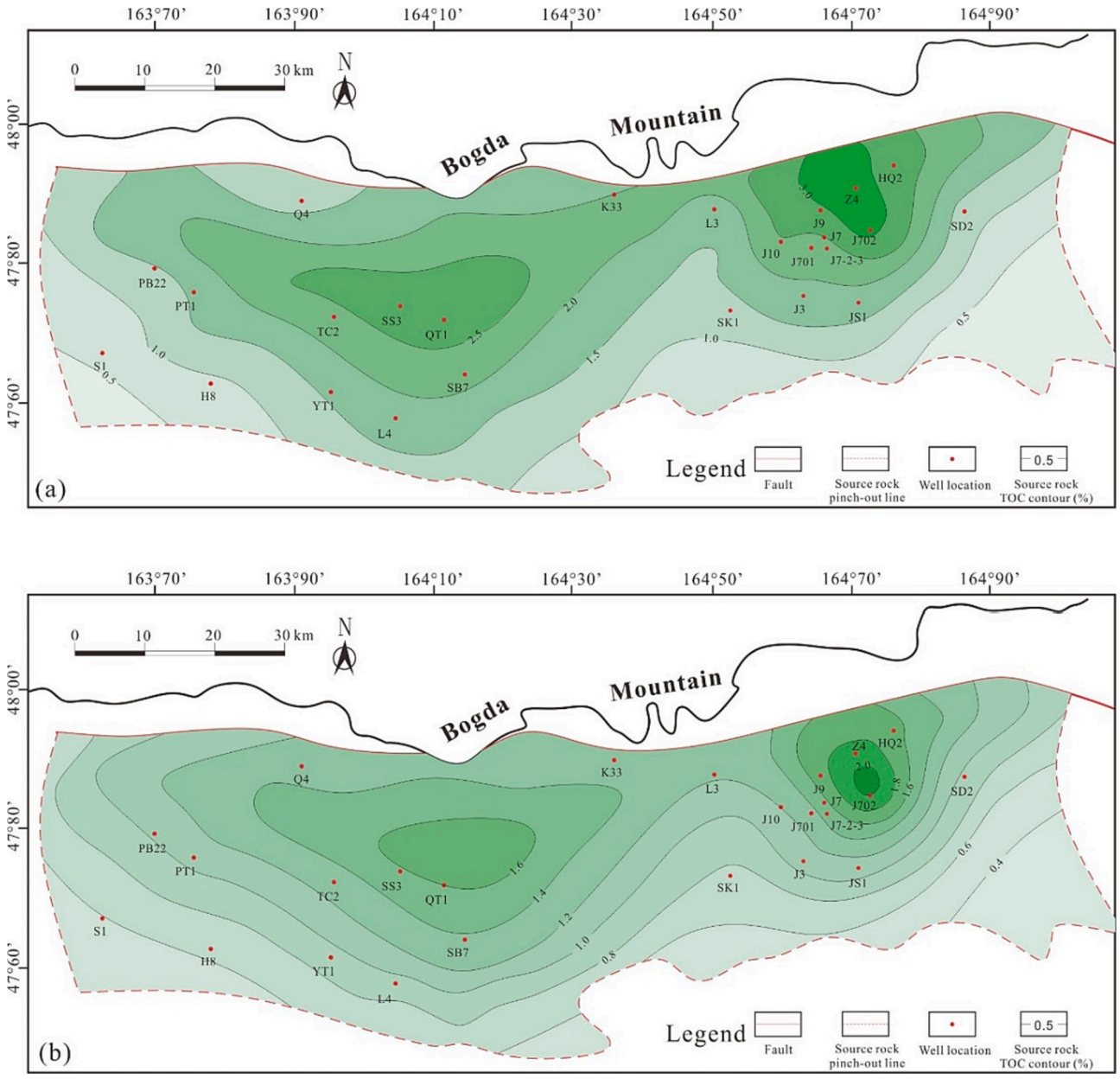

Fig. 6. The TOC contour map of the J_1s^2 source rocks (a) and the J_1s^1 source rocks (b) of the Sangonghe Formation in the Taibei Sag, Turpan-Hami Basin.

0.24 to 0.46 (avg. 0.31) and 0.25–0.54 (avg. 0.33), respectively. The P/Ti, Ba/Al, and Mn/Fe ratios of the Sangonghe Formation mudstones were 0.02–0.18 (avg. 0.06), 36.56–83.23 (avg. 60.27), and 0.002–0.0188 (avg. 0.0996), respectively.

4.2. Biomarker characteristics of oil-sand extract

The predominant biomarkers of Lower Jurassic oil-sand extract samples were normal alkanes. In the Total ion chromatogram (TIC) mass chromatogram, the distribution of the n-alkanes series of the crude oil samples was relatively complete, with the carbon number distribution range between nC_{13} and nC_{35} and the main peak carbon range between nC_{16} and nC_{26} (Fig. 11). The n-alkanes are dominated by low molecular weight homologues with a unimodal distribution and an apex in the early to moderate range of n-alkanes. The relative content of Pr and Ph of isoprene alkane in oil/extract samples is low. The Pr/Ph ratio in the J_1s^2 crude oil samples ranged from 1.49 to 2.58, with an average value of 1.99, indicating an oxic waterbody during sedimentation.

In the m/z=217 mass chromatogram, the ααα20RC_{29} regular sterane contents of the oil samples are relatively dominant, and the distribution pattern of the regular sterane ααα20RC_{27}-C_{28}-C_{29} in some samples shows an obvious asymmetric "V" shape, suggesting that the content of regular sterane ααα20RC_{27} is equivalent to that of ααα20RC_{29}. The ααα20RC_{27}/C_{29} ratio ranged from 0.82 to 0.92 (avg. 0.87), indicating that the source of crude oil had an obvious contribution from the aquatic organisms.

In the mass chromatogram with m/z=191, C_{30} hopane and C_{29} norhopane were dominant in most of the tested samples. In the J_1s oil/extract samples, a certain content of gammacerane was observed, with the GI ranging from 0.22 to 0.28 with an average value of 0.24, indicating its origin was the source rock that formed in a brackish water column.

4.3. Hydrocarbon generation and expulsion model

4.3.1. The establishment of hydrocarbon generation and expulsion model

The Eq. (1) from Li et al., (2020a) is used for fitting the model of the

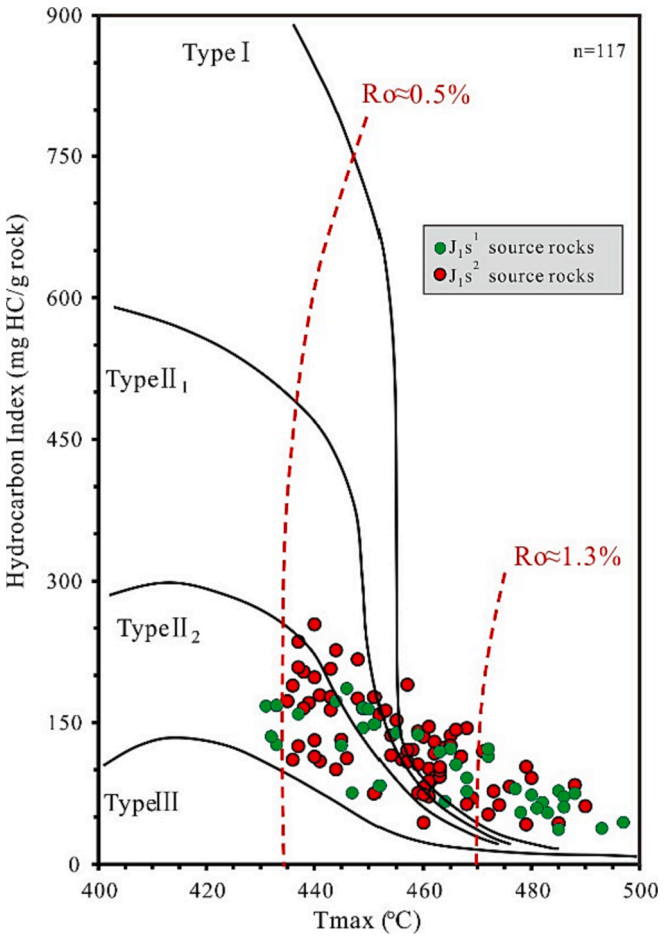

Fig. 7. Organic matter type characterized by hydrocarbon index (HI) and T_{max} of J_1s source rock in the Taibei Sag (according to Peters and Cassa (1994)).

plotted T_{max} and HI and their relationship is shown in Fig. 12. HI_0 was determined to be 279 and 211 mg HC/g TOC, respectively to best fit the variation trend of the samples from J_1s^2 and J_1s^1. The simulated curve covers the vacancy in the flat segment at both ends of the line to complete the entire thermal evolution process from the immature to mature stages (Fig. 12). The model of J_1s^2 samples has a steeper gradient in the middle part of the curve than that of the J_1s^1 because it possesses a much larger θ value, indicating that the source rock of J_1s^2 has experienced a more rapid hydrocarbon transformation than that of J_1s^1. The specific T_{max} value that corresponds to a large amount of kerogen transformation in the J_1s^2 model was lower than that in the J_1s^1 model. Thus the rapid hydrocarbon generation period of the J_1s^2 source rocks was earlier with a narrower hydrocarbon generation window than that of the J_1s^1. The main factors controlling this phenomenon are discussed in the following discussion sections.

The models in Fig. 12 can only express the feature of hydrocarbon generation. To comprehensively analyze the entire kinetic process, the simulated kinetic models are plotted in Figs. 13 and 14 by applying the expulsion formulas. The green dashed lines represent the thresholds at which hydrocarbon generation and expulsion began. The measured T_{max} was converted into Ro using Eq. (11) and is plotted in Fig. 13a to show the application of the conceptual model (Fig. 2) in a practical situation. The HET was determined by identifying the point at which the S_1+S_2/TOC value began to decrease as Ro increases, indicating that the source rocks began to expel hydrocarbons. The HET of the Ro of J_1s^1 and J_1s^2 source rocks was approximately 0.88 %.

The hydrocarbon generation potential of the source rock is a measure of the amount of organic matter converted into hydrocarbons. T_{re} determines when the hydrocarbon is discharged from the source rock, influencing the measurement of Q_e. When the degree of thermal evolution increases, the kerogen within the organic matter starts to decompose and convert into hydrocarbons. This leads to a consistent upward trend in T_r and Q_g values, representing a rapid hydrocarbon generation and transformation period, followed by a stabilization as thermal maturity continues to rise. For the J_1s^2 samples, when Ro was approximately 0.88 %, hydrocarbon expulsion began, and T_{re} was determined as 39.7 %. For the J_1s^1 samples, T_r and Q_g increased gradually during thermal evolution, however, within the limited maturity range, there was no obvious flattening was observed. By applying the same discrimination method, the T_{re} of the J_1s^1 source rocks was 29.1 %. The Q_g values corresponding to T_{re} were 111.20 and 59.94 mg HC/ g TOC, respectively.

The maturity of source rocks of the Sangonghe Formation in the Taibei Sag reached up to 1.20 % in the depression area. For the J_1s^2 source rocks, this evolution degree was close to the equilibrium end point of Q_g. If this Ro value (1.2 %) is assumed to be the maximum thermal evolution degree of the source rock, the maximum of Q_g and Q_e are 277.89 and 166.07 mg HC/ TOC, respectively, and the corresponding expulsion efficiency is 57.20 %. The degree of thermal evolution of the J_1s^1 source rocks in the Taibei Sag was similar to that of the J_1s^2, and the Q_g values of the J_1s^1 samples with the Ro of 1.20 % were far from reaching the climax. In this case, within the current maturity stage, the maximum of Q_g and Q_e of J_1s^1 source rocks was 154.87 and 94.03 mg HC/ TOC, respectively, and the maximum expulsion efficiency was 58.90 %.

4.3.2. *Hydrocarbon generation and expulsion intensities*

The calculation was completed by multiplying the integration results of Q_g or Q_e at different evolution stages of the source rock by the thickness, TOC, and rock density using Eq. (9) and (10). Contour maps of I_g and I_e of J_1s^1 and J_1s^2 source rocks are shown in Fig. 15, with two hydrocarbon generation and expulsion centers developed around wells QT1 and J7 in both members of the Sangonghe Formation.

The amount of hydrocarbon generated in the two sub-sags is close (Fig. 15). Source rock in the eastern sub-sag was larger in thickness and TOC content, resulting in a higher hydrocarbon generation intensity (maximum $I_g=120\times10^4 t/km^2$), but the distribution area was limited. Although the range of the hydrocarbon generation center of the J_1s^1 source rock was similar to that of J_1s^2, the hydrocarbon generation and expulsion intensity were nearly half lower than that of J_1s^2, with the highest value of the I_g and I_e centers migrating from east to west.

5. Discussion

This section discusses the sedimentary environment and organic matter input characteristics of both members of the Sangonghe Formation. A detailed oil-source correlation was used in combination with the characteristics of hydrocarbon source rocks and crude oil biomarkers to confirm the effectiveness of the J_1s source rocks in the Taibei Sag. In addition, this section discusses the influence of sedimentary environments and organic matter origin difference between the J_1s^1 and J_1s^2 source rocks on their geochemical characteristics, hydrocarbon generation and expulsion features.

5.1. *Depositional environment and source of organic matters*

5.1.1. *Palaeo-water depth and primary productivity*

The J_1s^2 mudstones were located at the top of the Sangonghe Formation and were deposited during a large-scale transgression (Fig. 1e), which resulted in the formation of continuous mudstone with a large thickness, characterized by a high gamma-ray logging response. Generally accepted is that the relative contents of the major elements Mn and Fe represent the depth of the water column (Liang et al., 2018). Therefore, the Mn/Fe ratio is larger in sediments formed in deeper water

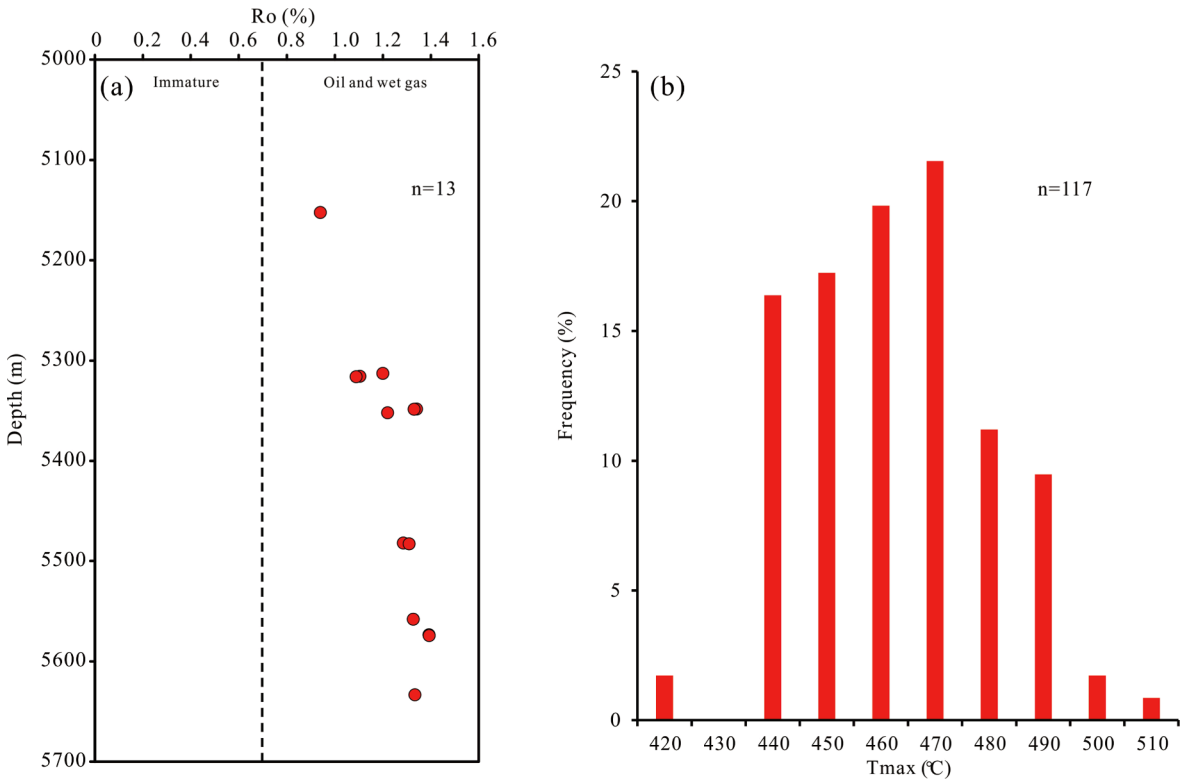

Fig. 8. Thermal evolution characteristics of J_1s source rocks in the Taibei Sag. (a). Relationship between Ro versus depth. (b). Frequency distribution histogram of T_{max}.

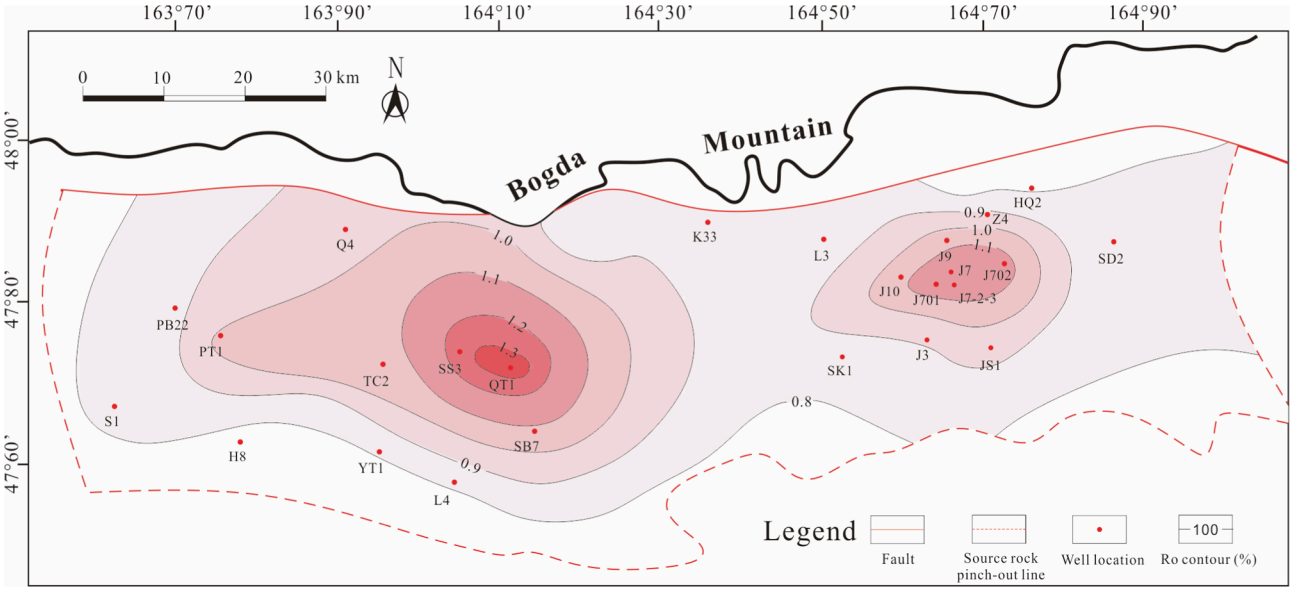

Fig. 9. The Ro contour map of the J_1s source rocks in the Taibei Sag, Turpan-Hami Basin.

bodies (Li et al., 2022). The mean value of the Mn/Fe ratio was higher in the J_1s^2 mudstones (0.0009–0.1675, avg. 0.0241) than in J_1s^1 (0.0056–0.0336, avg. 0.0134) (Fig. 16a). The ratio of (Al+Fe)/(Ca+Mg) is controlled by terrigenous materials and usually decreases with increasing depth of water (Li et al., 2022), and this ratio was lower in the J_1s^2 mudstones (2.70–32.07, avg. 18.16) than that in J_1s^1 (14.64–41.80, avg. 27.79) (Fig. 16b), therefore, the mudstones of J_1s^2 were formed in a deeper water body than that of J_1s^1.

Primary productivity is an important index to evaluate the enrichment of organic matter in fine-grained sediments (Li et al., 2020b; Li et al., 2022; Pan et al., 2020; Shen et al., 2015). Phosphorus is a necessary nutrient for biological growth and will settle in sediment after the organism is dead (Pan et al., 2020). Therefore, the relative P content in the sediment was strongly correlated with the primary productivity of the water column (Algeo and Maynard, 2004; Pan et al., 2020; Shen et al., 2014). The P/Ti of J_1s^2 samples ranged between 0.019 and 0.175 (avg. 0.060), higher than that of the J_1s^1 (0.016–0.020, avg. 0.047), indicating higher primary productivity during the deposition of J_1s^2

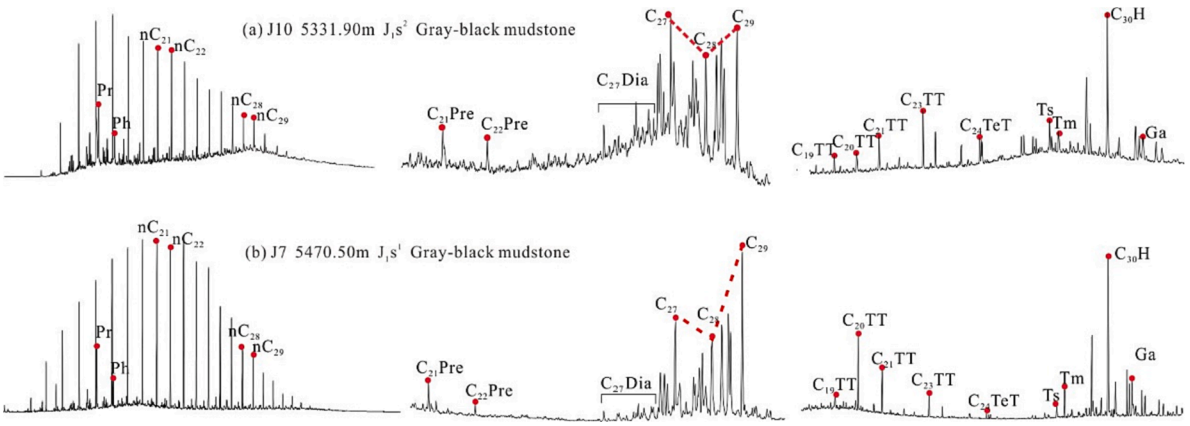

Fig. 10. GC-MS chromatograms showing distributions of total ion chromatograms (TIC) of saturated hydrocarbons, hopanes (*m/z* 191) and steranes (*m/z* 217) in the source rock samples of J_1s in the Taibei Sag, Turpan-Hami Basin. Pr and Ph are pristane and phytane respectively; the number at the top of the peak represents the carbon number of n-alkanes; Pre = Pregnane; Pro = Progesterone; $C_{30}H$ = C_{30} Hopane; Ga = Gammacerane; Pre = Pregnane; C_{27} - C_{29} are normal sterane ααα20RC_{27}-C_{29}.

Table 2
The concentration of trace element of mudstone samples from the upper and lower members of the Sangonghe Formation in the Taibei Sag (unit in μg/g). Trace element composition of the upper crust according to Taylor and McLennan (1985).

Sample ID	Member	Depth	Sample type	Sc	V	Cr	Co	Ni	Cu	Ga	Rb	Sr	Ba	Zr	Th	U
		(m)		(μg/g)												
W5	J_1s^2	5328.68	core sample	26.9	121.0	87.0	14.2	22.4	32.4	17.8	83.7	140.0	502.0	163.0	9.7	2.7
W11	J_1s^2	5331.90	core sample	16.5	99.5	115.0	15.2	21.5	34.4	19.9	105.0	126.0	542.0	204.0	11.0	3.4
W23	J_1s^2	5149.80	core sample	16.1	99.9	93.9	14.6	22.7	33.7	19.3	123.0	162.0	587.0	176.0	11.8	3.4
W25	J_1s^2	5152.62	core sample	16.4	96.9	84.1	14.4	22.4	33.7	19.4	92.0	128.0	562.0	173.0	9.2	3.0
W15	J_1s^2	5314.52	core sample	16.1	191.0	75.6	5.1	23.2	45.2	19.9	121.0	218.0	739.0	177.0	9.7	4.5
W17	J_1s^2	5315.72	core sample	24.1	145.0	77.1	9.0	23.5	52.9	26.0	195.0	216.0	842.0	229.0	12.9	5.1
W18	J_1s^2	5317.22	core sample	22.2	138.0	76.3	17.6	33.8	48.7	23.9	185.0	190.0	773.0	210.0	13.4	3.5
W19	J_1s^2	5318.02	core sample	21.1	116.0	69.6	19.4	30.0	42.0	21.4	144.0	176.0	664.0	207.0	11.2	3.1
W76	J_1s^2	4558.01	core sample	35.2	143.0	66.4	5.5	20.4	75.4	29.9	42.4	125.0	575.0	284.0	12.2	2.9
W77	J_1s^2	4559.58	core sample	23.4	117.0	51.8	9.8	26.4	49.7	28.3	62.6	125.0	513.0	304.0	7.4	2.5
W61	J_1s^2	5480.78	core sample	18.8	106.0	91.8	3.4	13.4	32.1	23.2	116.0	101.0	625.0	180.0	14.4	3.4
W62	J_1s^2	5481.38	core sample	20.1	106.0	81.4	24.7	41.1	47.5	25.2	88.4	115.0	542.0	225.0	11.4	3.7
W27	J_1s^1	5308.60	core sample	24.7	133.0	70.3	14.0	32.7	44.5	28.1	188.0	156.0	912.0	232.0	11.5	6.2
W110	J_1s^1	5572.47	core sample	19.0	105.0	69.7	12.4	21.1	42.0	23.3	141.0	147.0	819.0	236.0	9.9	2.8
W111	J_1s^1	5572.88	core sample	20.7	125.0	101.0	16.4	39.4	60.9	25.4	124.0	144.0	669.0	170.0	17.3	5.2
W115	J_1s^1	5574.61	core sample	23.4	138.0	60.0	6.5	16.4	43.3	33.8	103.0	105.0	875.0	246.0	7.8	2.1
W116	J_1s^1	5575.65	core sample	23.3	144.0	60.7	7.6	17.5	40.0	29.6	102.0	101.0	815.0	231.0	7.5	1.9
Upper crust				13.6	107.0	85.0	17.0	44.0	25.0	17.0	112.0	350.0	550.0	74.0	10.7	2.8

Table 3
The composition of major oxides (unit in wt%) of mudstone samples from the upper and lower members of the Sangonghe Formation in the Taibei Sag. Major oxides composition of the upper crust according to Taylor and McLennan (1985).

Sample ID	Member	Depth	Sample type	SiO_2	Al_2O_3	Fe_2O_3	MgO	CaO	Na_2O	K_2O	MnO	TiO_2	P_2O_5
		(m)		(%)									
W5	J_1s^2	5328.68	core sample	53.84	14.85	11.88	1.69	1.02	1.16	2.32	0.246	0.852	0.205
W11	J_1s^2	5331.90	core sample	62.32	17.44	4.28	1.04	1.14	1.68	2.81	0.074	1.020	0.122
W23	J_1s^2	5149.80	core sample	61.29	17.96	4.93	1.22	0.55	1.35	3.97	0.074	1.010	0.111
W25	J_1s^2	5152.62	core sample	59.92	16.55	6.58	1.21	1.07	1.39	2.50	0.105	0.943	0.132
W15	J_1s^2	5314.52	core sample	47.63	17.59	1.81	0.65	5.73	0.46	3.73	0.274	0.870	0.024
W17	J_1s^2	5315.72	core sample	59.44	22.43	3.67	1.29	0.09	0.54	5.58	0.021	0.957	0.054
W18	J_1s^2	5317.22	core sample	59.14	20.23	6.86	1.47	0.12	0.62	4.85	0.067	0.931	0.054
W19	J_1s^2	5318.02	core sample	58.55	18.82	8.46	1.45	0.19	0.89	4.40	0.102	0.970	0.089
W76	J_1s^2	4558.01	core sample	53.55	25.58	2.58	0.73	0.13	0.42	1.13	0.002	1.210	0.038
W77	J_1s^2	4559.58	core sample	57.74	24.54	3.48	0.88	0.13	0.31	1.63	0.007	1.370	0.044
W61	J_1s^2	5480.78	core sample	64.37	21.56	1.80	0.77	0.11	0.86	3.35	0.005	1.050	0.027
W62	J_1s^2	5481.38	core sample	60.06	20.48	5.01	1.40	0.17	0.51	2.68	0.037	1.220	0.062
W27	J_1s^1	5308.60	core sample	59.36	21.77	4.94	1.59	0.08	0.63	5.36	0.025	0.887	0.041
W110	J_1s^1	5572.47	core sample	62.81	18.29	5.26	1.35	0.42	0.85	4.16	0.159	1.220	0.202
W111	J_1s^1	5572.88	core sample	59.19	20.58	7.74	1.35	0.11	0.58	3.43	0.046	1.050	0.058
W115	J_1s^1	5574.61	core sample	54.36	25.24	5.48	0.64	0.15	0.36	3.13	0.060	1.120	0.025
W116	J_1s^1	5575.65	core sample	52.88	25.31	6.71	0.70	0.17	0.32	3.12	0.055	1.150	0.038
Uppercrust				66.00	15.20	–	2.20	4.20	1.60	3.90	0.080	0.410	0.150

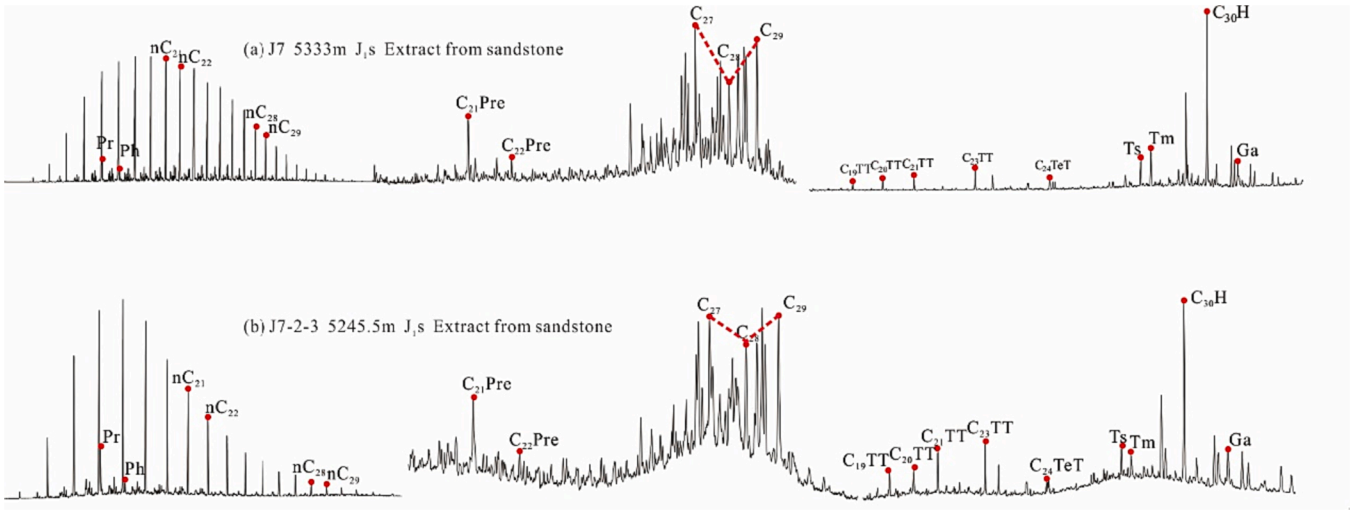

Fig. 11. GC-MS chromatograms showing distributions of total ion chromatograms (TIC) of saturated hydrocarbons, hopanes (*m/z* 191) and steranes (*m/z* 217) in the J_1s oil-sand extract samples in the Taibei Sag, Turpan-Hami Basin.

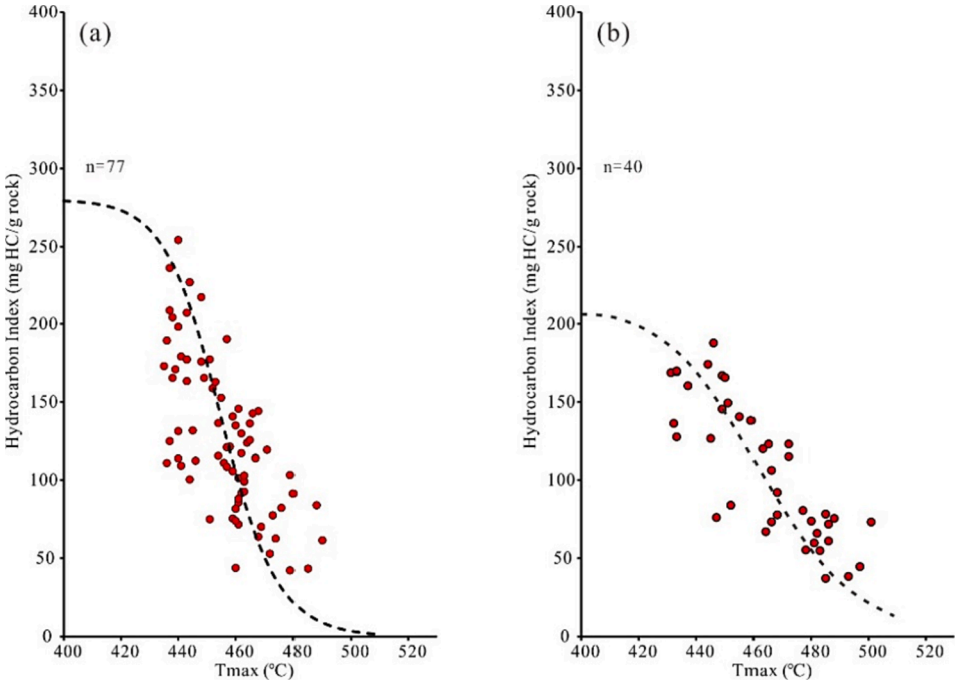

Fig. 12. Simulation model of hydrocarbon generation potential fitted by Rock-Eval data (HI versus T_{max}) of the J_1s^2 source rocks (a) and the J_1s^1 source rocks (b) in the Taibei Sag, Turpan-Hami Basin.

(Fig. 16c).

5.1.2. Redox condition and palaeosalinity

Pristane (Pr) and phytane (Ph) are commonly used for the discrimination of the sedimentary environment of the deposits and are detected in all source rock and oil/extract samples from the Sangonghe Formation. Phytanol can be converted into pristane under oxidation conditions, so the ratio of Pr/Ph is widely used as the indicator of the redox condition in the sedimentary environment. Generally, a low Pr/Ph ratio (<1) indicates an anoxic environment, and a Pr/Ph ratio > 3 indicates an oxidizing environment. (Didyk et al., 1978; Peters et al., 2005; Peters and Moldowan, 1993; Powell and McKirdy, 1973; Ten Haven et al., 1987). The distribution range of the Pr/Ph ratio of source rocks from both members was between 0.88 and 3.19, reflecting a weak oxidation environment (Fig. 17a).

Tricyclic terpenes and hopanes are ubiquitous in sediments and source rock extracts and can be used as important indicators for determining the biological origins and sedimentary environments (Degrande et al., 1993; Jin et al., 2019; Peters et al., 2005; Peters and Moldowan, 1993). Sinninghe Damsté et al. (1995) proposed gammacerane as an indicator of the stratification of water bodies, meanwhile the GI is often used to indicate the salinity of water bodies. The average GI values of the J_1s^2 and J_1s^1 source rocks were 0.27 and 0.23, respectively, indicating that both source rocks were formed in a brackish water column, and the GI values of the J_1s^2 samples were slightly higher than that of the J_1s^1 (Fig. 17a). Previous studies have pointed out that GI and Pr/Ph are usually negatively correlated, but this phenomenon is not obvious in this study (Chen and Summons, 2001; Mann et al., 1987; Sun et al., 2016), therefore, this may indicate that there is no interaction between water salinity and oxidation-reducibility.

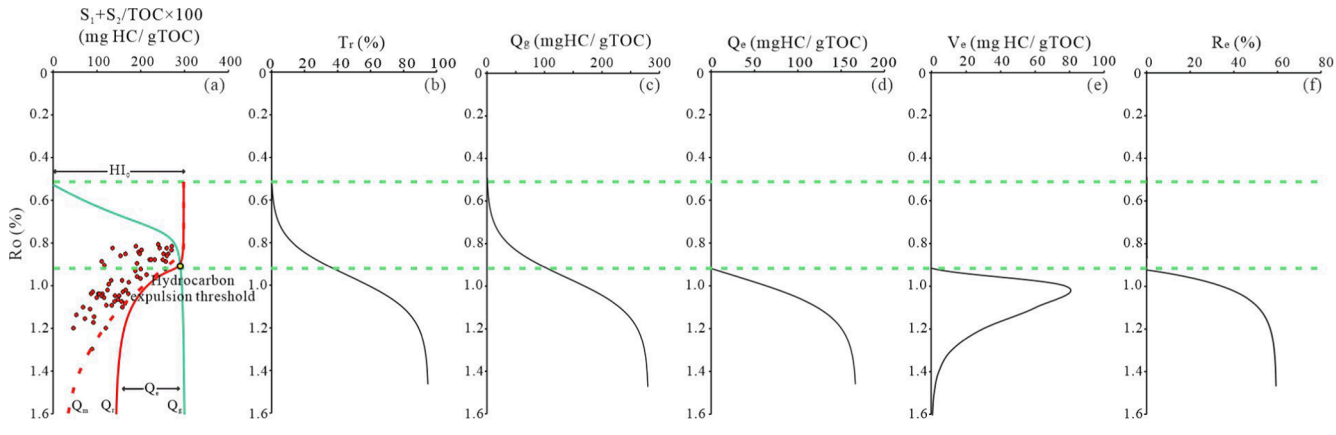

Fig. 13. Simulation model of hydrocarbon generation and expulsion characteristics of the J_1s^2 source rocks in the Taibei Sag, Turpan-Hami Basin.

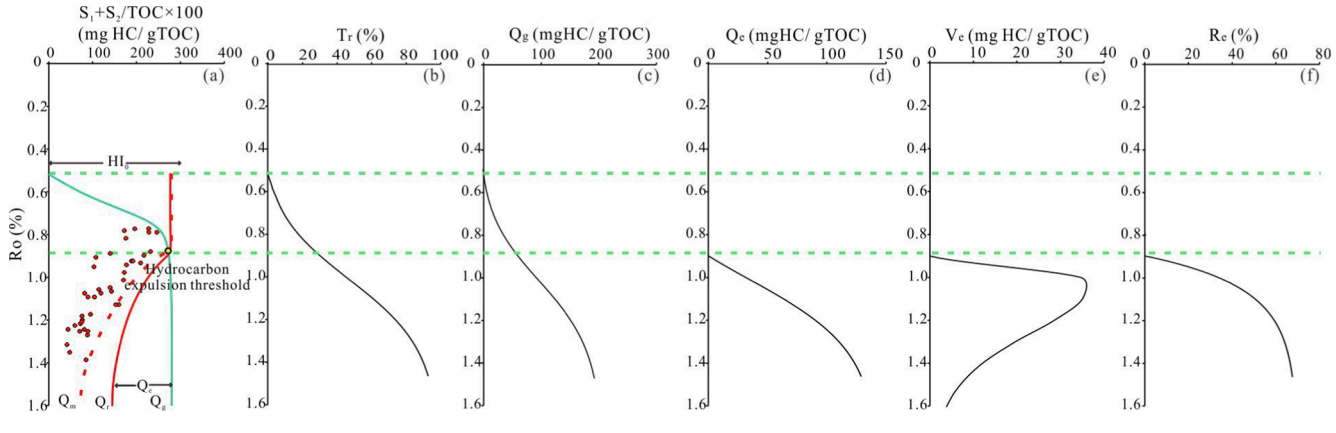

Fig. 14. Simulation model of hydrocarbon generation and expulsion characteristics of the J_1s^1 source rocks in the Taibei Sag, Turpan-Hami Basin.

The contents of trace elements Sr and Ba are commonly used for restoring the palaeosalinity of the water column (Custodio, 2002; Pan et al., 2020; Rohling, 2000; Zheng et al., 2022). Therefore, salinity assessment can be effectively accomplished using Sr/Ba ratio (Zhang et al., 2018). Specifically, a ratio within the following ranges indicates different water conditions: $>$ 0.5 for saltwater, 0.2–0.5 for brackish water, and $<$ 0.2 for freshwater (Wei and Algeo, 2020; Zheng et al., 2022). The distribution range of the Sr/Ba ratio of samples from J_1s^1 and J_1s^2 reflects a brackish water condition. The Sr/Ba ratio of sediments from J_1s^2 is higher than that of J_1s^1. This observation aligns with the earlier statement regarding the GI, indicating that the salinity of the water column during the deposition of J_1s^2 was higher than that of J_1s^1 (Fig. 17b).

The relative contents of trace elements Ni and Co can effectively reflect the degree of redox conditions in water bodies during sedimentation with a higher Ni/Co ratio indicating a reducing environment (Elderfield and Greaves, 1982; Wang et al., 2022a). Generally, the Ni/Co ratios in the ranges of $<$ 5, 5–7, and $>$ 7 represent oxidizing, oxygen-poor, and anoxic environments, respectively (Elderfield and Greaves, 1982; Wang et al., 2022a). The ratio of U/Th $<$ 0.75 and V/Cr $<$ 2 represent an oxic condition (Jones and Manning, 1994; Pan et al., 2020; Li et al., 2022). Thus, the redox conditions during the sedimentation of the source rocks in both members of the Sangonghe Formation were similar, and both were deposited in an oxidizing environment (Table 2, Fig. 17b, c).

5.1.3. Source of organic matters

High-carbon n-alkanes after C_{22} generally originate from terrestrial organisms, and low-carbon n-alkanes before C_{21} mainly originate from aquatic organisms and microorganisms, therefore, the normal-alkane distribution and the ratio of n-alkane C_{21-}/C_{22+} are widely used to determine the origin of organic matter (Peters and Moldowan, 1993). Steroidal compounds in sediments are commonly found in prokaryotic microbial organisms, such as plankton, aquatic organisms, terrestrial plants, higher animals, and bacteria (Philp and Gilbert, 1986). The C_{27}-C_{28}-C_{29} steranes are derivatives of sterols that can be used to study the provenance, maturity, and sedimentary environment of crude oil and source rocks (Peters and Moldowan, 1993). Studies have shown that C_{27} regular steranes are mainly derived from zooplankton, C_{28} from phytoplankton, and C_{29} from terrigenous plants, brown algae, and other green algae (Huang and Meinschein, 1979; Moldowan et al., 1985). GC-MS analysis showed a higher ratio of normal alkane $C_{21-}/C_{22+}$and a higher content of ααα20RC_{27} regular sterane in samples from J_1s^2 than that in the J_1s^1, indicating a higher proportion of aquatic organism contribution to the source rocks during the deposition of the J_1s^2 source rocks than that of J_1s^1 (Fig. 18a, b).

5.2. Oil-source correlation of the Sangonghe Formation

The spectrogram from GC-MS analysis of the lower Jurassic crude oil/extract samples shows very little UCM (Unresolved Complex Mixture) bulge, and the n-alkane distribution of the J_1s oil/extract sample in the study area was relatively complete. These collectively suggest that there is a low degree of biodegradation molecular isomerization of organic compounds (Liu et al., 2022). Therefore, the distribution of the biomarker parameters of the oil/extract can effectively reflect the origin of the organic matter.

Nearly equal contents of regular sterane ααα20RC_{27} and ααα20RC_{29}

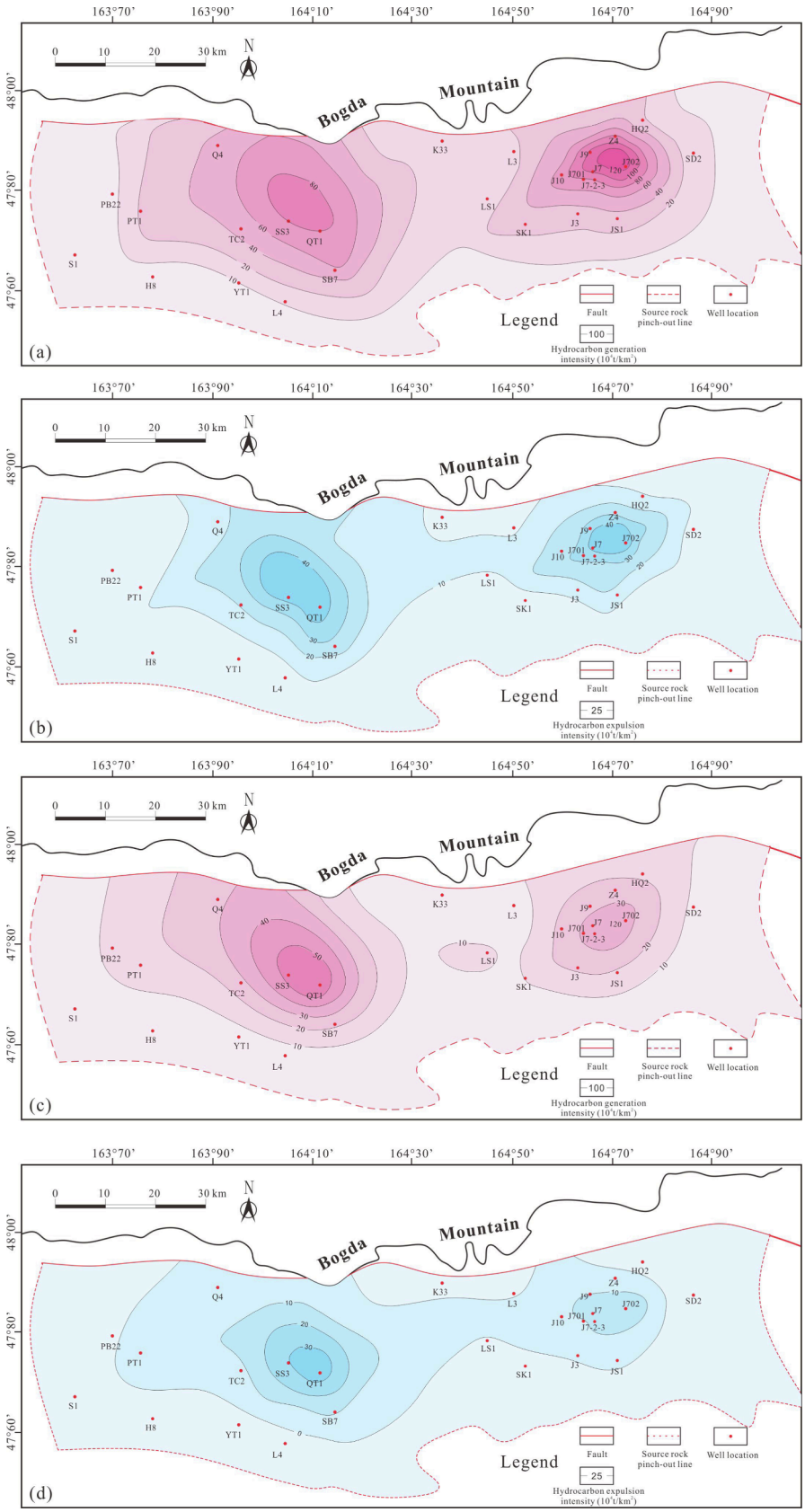

Fig. 15. Hydrocarbon generation and expulsion intensities of J_1s source rocks in the Taibei Sag, Turpan-Hami Basin; (a) Hydrocarbon generation intensity (I_g) of J_1s^2 source rocks; (b) Hydrocarbon expulsion intensity (I_e) of J_1s^2 source rocks; (c) Hydrocarbon generation intensity (I_g) of J_1s^1 source rocks; (d) Hydrocarbon expulsion intensity (I_e) of J_1s^1 source rocks.

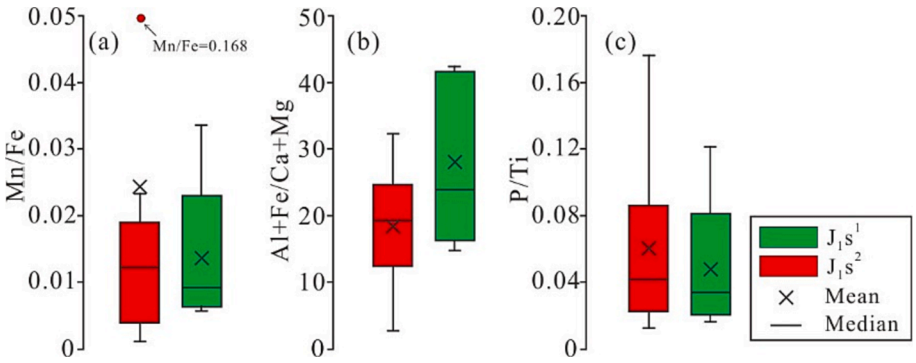

Fig. 16. Distribution histograms of Mn/Fe, Al+Fe/Ca+Mg and P/Ti ratios of source rock samples from both members of the Sangonghe Formation in the Taibei Sag, Turpan-Hami Basin.

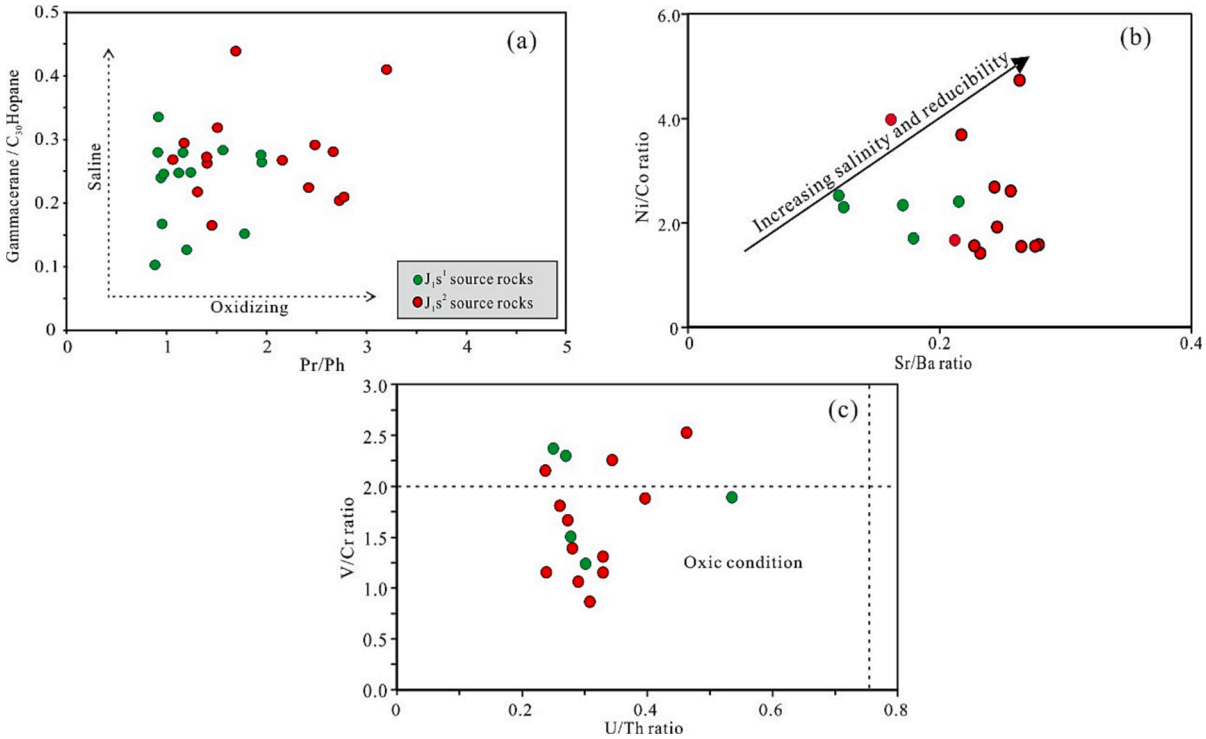

Fig. 17. Correlation diagrams between the Gammacerane/C_{30}Hopane and Pr/Ph ratios (a), Ni/Co ratio and Sr/Ba ratios (b), and V/Cr ratio and U/Th ratios (c) of source rock samples from both members of the Sangonghe Formation in the Taibei Sag, Turpan-Hami Basin.

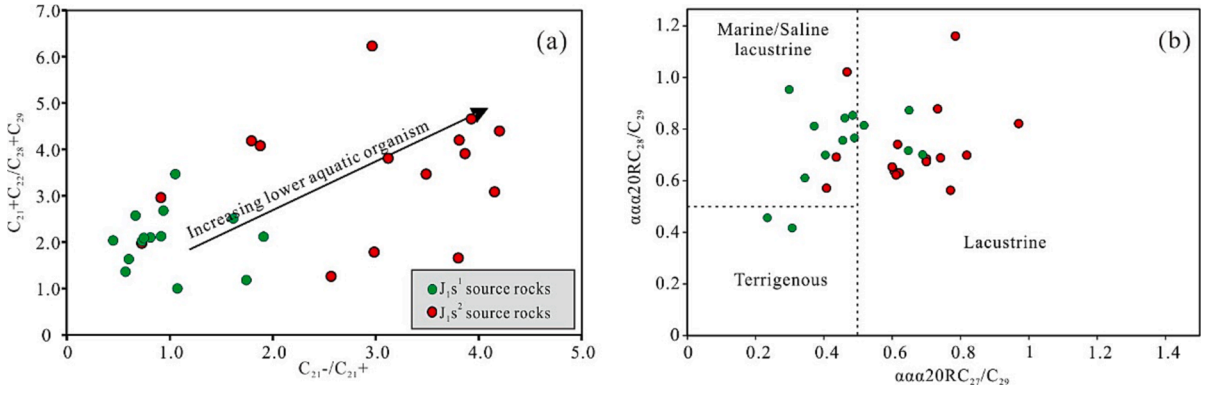

Fig. 18. Correlation diagrams between the C_{21}+C_{22}/C_{28}+C_{29} and C_{21-}/C_{21+} ratios (a), ααα20RC_{28}/C_{29} versus ααα20RC_{27}/C_{29} (b) of source rock samples from both members of the Sangonghe Formation in the Taibei Sag, Turpan-Hami Basin.

with a certain amount of gammacerane in the oil/extract samples reflect its origin from lacustrine mudstone that formed in a brackish water sedimentary environment, with a certain contribution from low aquatic organisms. The specific biomarker parameters of this type of oil were plotted in the same area as those of the J_1s^2 samples as shown in Fig. 19. Additionally, their spectrogram distribution were highly similar (Figs. 10, 11), indicating that the oil in the Sangonghe Formation was sourced from the J_1s source rocks, and the contribution of the J_1s^1 source rocks could not be excluded. Studies have suggested that the petroleum in the existing reservoirs was contributed by coaly source rocks from the Badaowan Formation, which is characterized by a high Pr/Ph ratio and an extremely low GI among biomarkers (He et al., 2022). The plotted biomarker parameters of the J_1b source rocks and J_1s oil samples were separated from each other in Fig. 19, indicating that the tested J_1s oil samples are not relevant to the contribution of the J_1b coaly source rocks.

5.3. *Hydrocarbon generation and expulsion comparison and analysis of controlling factors*

The kinetic parameter patterns established based on the existing hydrocarbon generation model of the J_1s^1 and J_1s^2 samples are displayed together to highlight their differences (Fig. 20a-e). The fitting curve of J_1s^2 source rocks has a higher HI_0 with a steeper slope represented by a higher β value and results in a narrower distribution of hydrocarbon generation window than J_1s^1 source rocks, indicating that more kerogen has been converted into hydrocarbons in an equal time interval (Fig. 20a). The relationship between the T_r and thermal maturity (Fig. 20b) reflects a more rapid increase of T_r and a higher value of T_{max} corresponding to the beginning of hydrocarbon generation of the J_1s^2 source rocks, indicating that a higher activating energy for kerogen decomposition is needed than that of the J_1s^1 samples. The duration of the hydrocarbon generation window and the energy needed to activate kerogen decomposition are significantly influenced by the uniformity of maceral compositions (Chen and Jiang, 2015). It can be concluded that the maceral composition of J_1s^1 source rock is more complex compared to that of J_1s^1. This interpretation is consistent with the GC-MS analysis results. The higher ratio of normal alkane $C_{21-}/C_{22+}$and ααα20RC_{27}/C_{29} of J_1s^2 source rocks are higher than those of the J_1s^1 source rocks. This suggests a higher proportion of aquatic organism contribution to the J_1s^2 source rocks than that of the J_1s^1. The sapropelic components in J_1s^2 source rocks minimized the complexity of macerals resulting from the terrigenous input.

The J_1s^2 source rocks have a higher I_g than those of J_1s^1, although their thickness and thermal maturity distributions are similar. The J_1s^2 source rock exhibited higher TOC and HI_0 than J_1s^1 source rock for several reasons: Firstly, from the perspective of sedimentation, the J_1s^2 mudstones were deposited during the lacustrine flood period, providing a more stable condition. Conversely, the J_1s^1 mudstones were deposited in a shore-shallow lacustrine environment within the intermittent period of the deltaic system, characterized by a substantial influx of terrigenous material. The influx significantly diluted the abundance of organic matter and introduced more higher plant organic input, leading to lower values of TOC and HI. Secondly, trace element analysis showed that the J_1s^2 source rock was deposited in a water body with slightly higher salinity than that of J_1s^1, which favored the preservation of organic matter in the sediment. The higher HI_0 can lead to a higher Q_g at the same transformation ratio. Collectively, these factors contribute to a higher calculated I_g value of the J_1s^2 source rocks.

Studies have shown that the hydrocarbon expulsion capacity of source rocks is related to TOC, hydrocarbon generation capacity, and thermal maturity, and that high-quality source rocks with higher TOC and better organic matter types usually have a better hydrocarbon expulsion capacity (Cooles et al., 1986; Eseme et al., 2007; Pepper, 1991; Pepper and Corvi, 1995; Ritter, 2003; Sun et al., 2021; Wilhelms et al., 1990). Although the J_1s^2 source rocks have higher TOC and better organic matter types than the J_1s^1 source rocks do, the hydrocarbon expulsion efficiency of the former is lower than the latter (Fig. 20e). When the hydrocarbon expulsion started, the corresponding T_{re} of J_1s^1source rocks 29.1 %, smaller than that of the J_1s^2 (T_{re}=39.7 %) (Fig. 20d), and the Q_g of J_1s^2 source rocks corresponding to T_{re} was 111.2 mg HC/ TOC, twice as large as that of the J_1s^1 source rocks (Q_g=59.94 mg HC/ TOC). These results indicate that a certain amount of hydrocarbons in the J_1s^1 source rock could have been expelled even if a relatively small proportion of kerogen had been decomposed. The most likely explanation for this phenomenon is the difference in the single-layer thickness and source-reservoir combination types of the two sets of source rocks.

Studies have reported the differences in hydrocarbon expulsion efficiency of source rocks with different thicknesses (Leythaeuser et al., 1988; Leythaeuser et al., 1984). The study of Mackenzie et al. (1988) indicates that the charging capacity of hydrocarbons would be higher in the interfaces between the source rocks and interbedded sandstones. The difference in the sedimentary environment leads to different single-layer thicknesses of the mudstone of J_1s^2 and J_1s^1. The J_1s^2 source rocks possess large and continuous thickness, effectively acting as a barrier to the migration of generated hydrocarbons. This impedes the hydrocarbon expulsion process, ultimately leading to lower R_e values. Conversely, J_1s^1 mudstones with limited thickness created better conditions for the generated hydrocarbons to discharge from the edge of the mudstones and resulted in a higher R_e compared to the J_1s^2 mudstones (Fig. 20e).

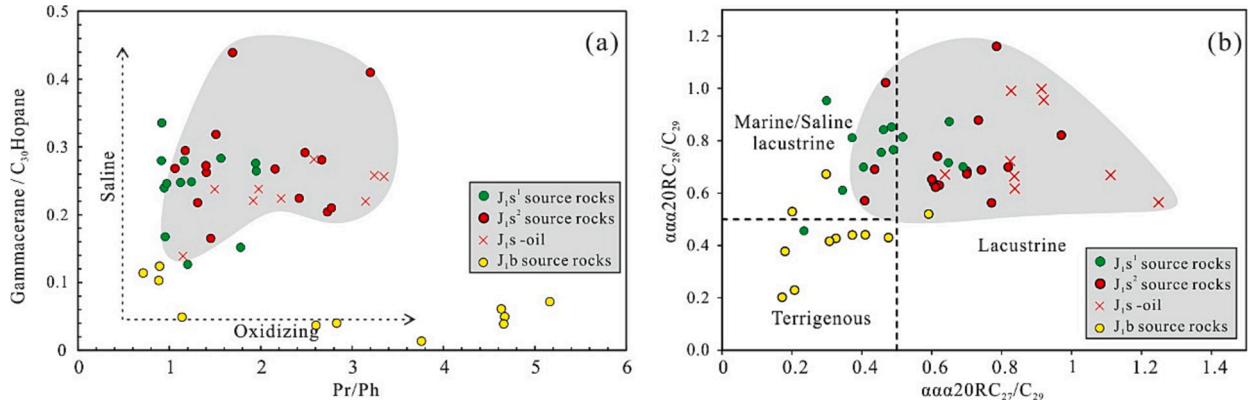

Fig. 19. Cross plots of oil-source correlation between J_1s oil-sand extracts and Lower Jurassic source rocks in the Taibei Sag, Turpan-Hami Basin. (a) Gammacerane/C_{30}Hopane versus Pr/Ph. (b) ααα20RC_{28}/C_{29} versus ααα20RC_{27}/C_{29}. The sample points of oil are distributed in the same range as the J_1s source rocks.

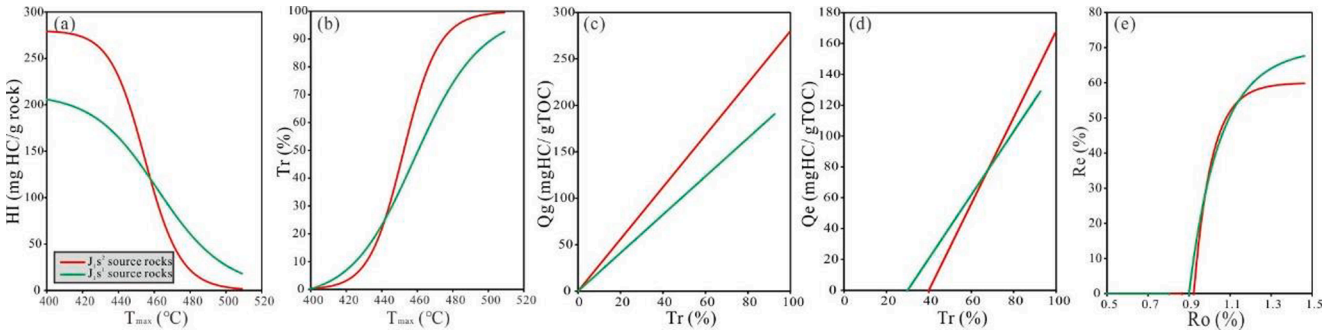

Fig. 20. Comparison of hydrocarbon generation and expulsion characteristics of J_1s^1 and J_1s^2 source rocks in the Taibei Sag, Turpan-Hami Basin; (a) HI versus T_{max}; (b) Transformation ratio (T_r) versus T_{max}; (c) Q_g versus T_r; (d) Q_e versus T_r; (e) Hydrocarbon expulsion efficiency (R_e) versus Ro.

5.4. Influence mechanism of sedimentary backgrounds on hydrocarbon generation and expulsion

During the deposition of the lower member of the Sangonghe Formation (J_1s^1), the mudstone was deposited in shore-shallow lacustrine environment under a deltaic sedimentary system, and the water body was relatively shallow and easily influenced by repeated river input (Fig. 21a). As a result, the mudstone was formed in a shallow water body and was limited in thickness. A large amount of terrigenous input during this period not only greatly diluted the abundance of organic matter but also complicated the maceral composition of the kerogens, resulting in a lower HI_0 and a wider range of hydrocarbon generation window. The limited thickness of the mudstone was conducive to the hydrocarbon expulsion process and led to a higher hydrocarbon expulsion efficiency.

During the deposition of the upper member of the Sangonghe Formation (J_1s^2), the lake expanded and maximum transgression occurred, and the depositional environment here evolved into a semi-deep to deep lacustrine environment which favored the development of thick and continuous mudstones (Fig. 21b). During this period, the water body is stable and the salinity is higher than that of the J_1s^1, which was conducive to the preservation of organic matter, resulting in a higher TOC of the mudstones. The semi-deep to deep lacustrine environment with higher primary productivity promoted the growth of aquatic organisms, thus enhancing the hydrocarbon generation potential and

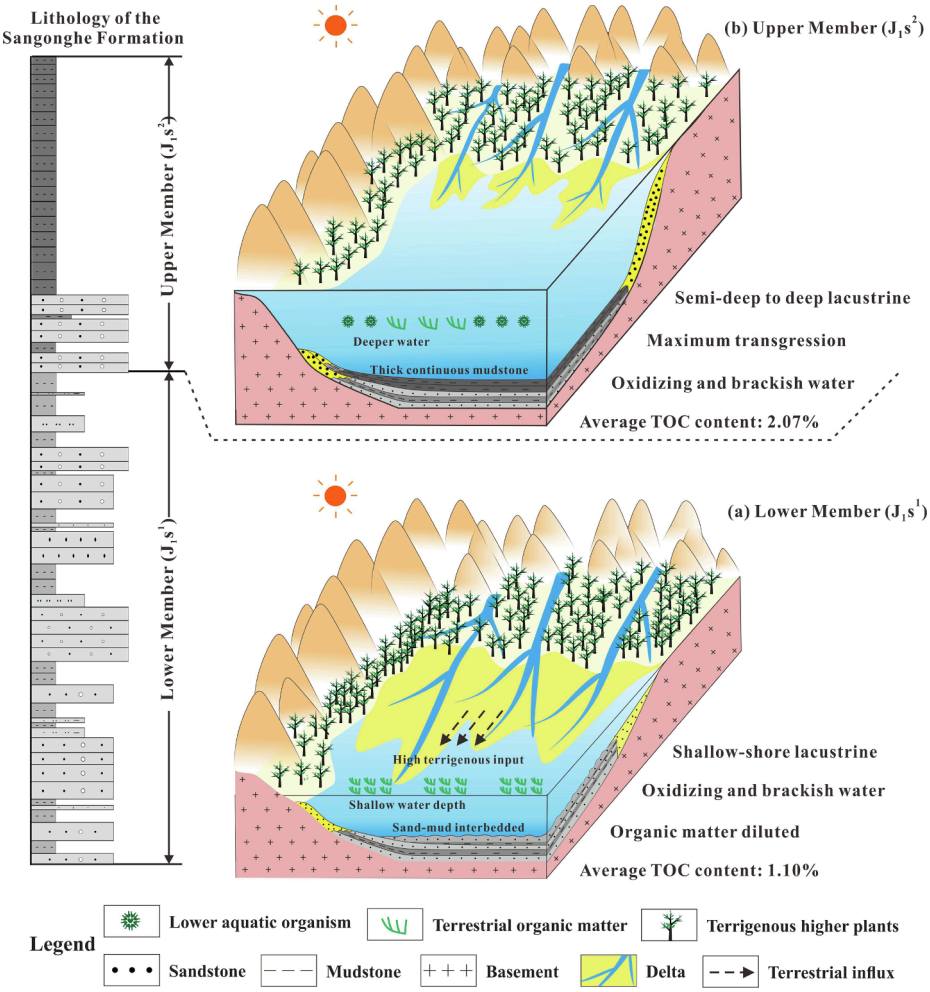

Fig. 21. The different sedimentary settings of the upper and lower members of the Sangonghe Formation in the Taibei Sag, Turpan-Hami Basin.

transformation rate. However, thick mudstone can block the migration of generated hydrocarbons and hinder the hydrocarbon expulsion process, resulting in a lower hydrocarbon expulsion efficiency. The calculated results of the accumulative hydrocarbon generation of the Sangonghe Formation in Taibei Sag matched the current exploration status, affirming the method's suitability for the study area.

6. Conclusions

(1) Oil-source correlation has confirmed that the hydrocarbons generated from the J_1s lacustrine mudstones have contributed to the existing Lower Jurassic tight oil reservoirs in Taibei Sag, Turpan-Hami Basin.
(2) During the maximum transgression period of J_1s^2. The stable water body with higher salinity and primary productivity leads to the mudstones containing a higher abundance of organic matter. There is a significant contribution of aquatic organisms in the maceral composition, leading to higher values of HI_0 and T_r of the J_1s^2 source rocks.
(3) The J_1s^1 mudstones were deposited in a shore-shallow lacustrine environment under the deltaic sedimentary system, with relatively shallow waterbody. The frequent fluvial activities introduced a substantial amount of terrigenous input, which greatly diluted the abundance of organic matter and complicated the maceral composition of the J_1s^1 mudstones. This further leads to a wider hydrocarbon generation window (lower T_r) and a lower Q_e. The interbedded thin-layer of mudstone exhibited higher hydrocarbon expulsion efficiency.

CRediT authorship contribution statement

Boran Wang: Software, Investigation, Writing – original draft. **Zhilong Huang:** Conceptualization, Methodology. **Dongsheng Xiao:** Data curation. **Haiyue Yu:** Data curation. **Wenren Zeng:** Supervision. **Xin Wang:** Writing – review & editing. **Tong Qu:** Writing – review & editing. **Zhiyuan Li:** Experiments, review & editing. **Yizhuo Yang:** Experiments, review & editing.

Declaration of Competing Interest

The authors declare that they have no known competing financial interests or personal relationships that could have appeared to influence the work reported in this paper.

Data availability

Data will be made available on request.

Acknowledgement

This work is financially supported by the Tuha Oilfield Company of China National Petroleum Corporation (CNPC)-China University of Petroleum (Beijing) Cooperation Science and Technology Project (Grant No. YJYHZC2022-044). The authors sincerely thank the Tuha Oilfield Company of China National Petroleum Corporation (CNPC) for providing core samples and some of the geologic data. The research was supported by State Key Laboratory of Petroleum Resources and Prospecting, China University of Petroleum (Beijing) and Beijing Institute of Nuclear Industry Geology.

Appendix A. Supplementary data

Supplementary data to this article can be found online at https://doi.org/10.1016/j.jseaes.2023.105911.

References

Algeo, T.J., Maynard, J.B., 2004. Trace-element behavior and redox facies in core shales of Upper Pennsylvanian Kansas-type cyclothems. Chem. Geol. 206, 289–318.
Chen, Z., Jiang, C., 2015. A data driven model for studying kerogen kinetics with application examples from Canadian sedimentary basins. Mar. Pet. Geol. 67, 795–803. https://doi.org/10.1016/J.MARPETGEO.2015.07.004.
Chen, J., Summons, R., 2001. Complex patterns of steroidal biomarkers in Tertiary lacustrine sediments of the Biyang Basin, China. Org Geochem. 32 (1), 115–126. https://doi.org/10.1016/S0146-6380(00)00145-5.
Cooles, G., Mackenzie, A., Quigley, T., 1986. Calculation of petroleum masses generated and expelled from source rocks. Org Geochem. 10 (1–3), 235–245. https://doi.org/10.1016/0146-6380(86)90026-4.
Custodio, E., 2002. Aquifer overexploitation: what does it mean? Hydrgeol. J. 10, 254–277.
Degrande, S., Aquinoneto, F., Mello, M., 1993. Extended tricyclic terpanes in sediments and petroleums. Org Geochem. 20 (7), 1039–1047. https://doi.org/10.1016/0146-6380(93)90112-O.
Didyk, B., Simoneit, B., Brassell, S., Eglinton, G., 1978. Organic geochemical indicators of palaeoenvironmental conditions of sedimentation. Nature 1978 272:5650, 272 (5650), 216–222. Doi: 10.1038/272216a0.
Dow, W., 1977. Kerogen studies and geological interpretations. J. Geochem. Explor. 7 (C), 79–99. https://doi.org/10.1016/0375-6742(77)90078-4.
Elderfield, H., Greaves, M., 1982. The rare earth elements in seawater. Nature 1982 296: 5854, 296(5854), 214–219. Doi: 10.1038/296214a0.
Eseme, E., Littke, R., Krooss, B., Schwarzbauer, J., 2007. Experimental investigation of the compositional variation of petroleum during primary migration. Org Geochem. 38 (8), 1373–1397. https://doi.org/10.1016/j.orggeochem.2007.03.003.
Feng, Y., Huang, Z., Wang, E., Zhang, H., Li, T., Liang, Y., 2021. The hydrocarbon generation and expulsion features of source rocks and tight oil potential of the second member of the Qiketai Formation, Shengbei area in the Turpan-Hami Basin, NW China. Geol. J. 56 (1), 337–358. https://doi.org/10.1002/GJ.3963.
Freund, H., Clouse, J., Otten, G., 1993. The effect of pressure on the kinetics of kerogen pyrolysis. Energy Fuels 7 (6), 1088–1094.
Gong, D., Cao, Z., Ni, Y., Jiao, L., Yang, B., Zhao, L., 2016. Origins of Jurassic oil reserves in the Turpan-Hami Basin, northwest China: evidence of admixture from source and thermal maturity. J. Pet. Sci. Eng. 146, 788–802. https://doi.org/10.1016/J.PETROL.2016.07.025.
He, H., Liang, S., Guo, X., Luo, Q., Wang, J., Chen, X., Yang, F., Xiao, D., Zhang, H., 2022. New discoveries and exploration prospects of middle and Lower Jurassic lithologic reservoirs in depression area of Turpan-Hami Basin China. J. Natural Gas Geosci. 7 (5), 265–275. https://doi.org/10.1016/J.JNGGS.2022.10.002.
Huang, W., Meinschein, W., 1979. Sterols as ecological indicators. GeochimicaEt Cosmochimica Acta 43 (5), 739–745. https://doi.org/10.1016/0016-7037(79)90257-6.
Inan, S., Yalçin, M., Mann, U., 1998. Expulsion of oil from petroleum source rocks: Inferences from pyrolysis of samples of unconventional grain size. Org Geochem. 29 (1–3–3 pt 1), 45–61. https://doi.org/10.1016/S0146-6380(98)00091-6.
Jarvie, D., Hill, R.J., Ruble, T.E., Pollastro, R., 2007. Unconventional shale-gas systems: The Mississippian Barnett Shale of north-central Texas as one model for thermogenic shale-gas assessment. AAPG Bull. 91 (4), 475–499. https://doi.org/10.1306/12190606068.
Jin, X., Zhang, Z., Wu, J., Zhang, C., He, Y., Cao, L., Zheng, R., Meng, W., Xia, H., 2019. Origin and geochemical implication of relatively high abundance of 17α (H)-diahopane in Yabulai basin, northwest China. Mar. Pet. Geol. 99, 429–442. https://doi.org/10.1016/J.MARPETGEO.2018.10.048.
Jones, B., Manning, D., 1994. Comparison of geochemical indices used for the interpretation of palaeoredox conditions in ancient mudstones. Chem. Geol. 111 (1–4), 111–129. https://doi.org/10.1016/0009-2541(94)90085-X.
Kuhn, P., di Primio, R., Hill, R., Lawrence, J., Horsfield, B., 2012. Three-dimensional modeling study of the low-permeability petroleum system of the Bakken formation. AAPG Bull. 96, 1867e1897.
Lafargue, E., Espitalie, J., Jacobsen, T., Eggen, S., 1990. Experimental simulation of hydrocarbon expulsion. Org Geochem. 16 (1–3), 121–131. https://doi.org/10.1016/0146-6380(90)90032-U.
Leila, M., Awadalla, A., Farag, A., Moscariello, A., 2022. Organic geochemistry and oil-source rock correlation of the Cretaceous succession in West Wadi El-Rayan (WWER) concession: Implications for a new Cretaceous petroleum system in the north Western Desert Egypt. J. Petrol. Sci. Eng. 219 (July), 111071 https://doi.org/10.1016/j.petrol.2022.111071.
Leythaeuser, D., Radke, M., Schaefer, R., 1984. Efficiency of petroleum expulsion from shale source rocks. Nature 1984 311:5988, 311(5988), 745–748. Doi: 10.1038/311745a0.
Leythaeuser, D., Schaefer, R., Radke, M., 1988. Geochemical effects of primary migration of petroleum in Kimmeridge source rocks from Brae field area, North Sea. I: Gross composition of C15+-soluble organic matter and molecular composition of C15+-saturated hydrocarbons. Geochim. Cosmochim. Acta 52 (3), 701–713. https://doi.org/10.1016/0016-7037(88)90331-6.
Li, T., Huang, Z., Feng, Y., Chen, X., Ma, Q., Liu, B., Guo, X., 2020c. Reservoir characteristics and evaluation of fluid mobility in organic-rich mixed siliciclastic-carbonate sediments: a case study of the lacustrine Qiketai Formation in Shengbei Sag, Turpan-Hami Basin, Northwest China. J. Pet. Sci. Eng. 185, 106667 https://doi.org/10.1016/J.PETROL.2019.106667.
Li, Y., Liu, G., Song, Z., Zhang, B., Sun, M., Tian, X., Yang, D., Wang, Y., Zhu, L., Cao, Y., 2022. Organic matter enrichment due to high primary productivity in the deep-water shelf: Insights from the lower Cambrian Qiongzhusi shales of the central

Sichuan Basin, SW China. J. Asian Earth Sci. 239 (September), 105417 https://doi.org/10.1016/j.jseaes.2022.105417.
Li, C., Pang, X., Huo, Z., Wang, E., Xue, N., 2020a. A revised method for reconstructing the hydrocarbon generation and expulsion history and evaluating the hydrocarbon resource potential: Example from the first member of the Qingshankou Formation in the Northern Songliao Basin, Northeast China. Mar. Petrol. Geol. 121, 104577 https://doi.org/10.1016/J.MARPETGEO.2020.104577.
Li, Q., Wu, S., Xia, D., You, X., Zhang, H., Lu, H., 2020b. Major and trace element geochemistry of the lacustrine organic-rich shales from the Upper Triassic Chang 7 Member in the southwestern Ordos Basin, China: Implications for paleoenvironment and organic matter accumulation. Mar. Pet. Geol. 111, 852–867. https://doi.org/10.1016/J.MARPETGEO.2019.09.003.
Liang, C., Wu, J., Jiang, Z., Cao, Y., Song, G., 2018. Sedimentary environmental controls on petrology and organic matter accumulation in the upper fourth member of the Shahejie Formation (Paleogene, Dongying depression, Bohai Bay Basin, China). Int. J. Coal Geol. 186, 1–13.
Liu, B., Huang Z., Luo Q., Chen X., Ma J., Wang M., 2012. Accumulation mode and resource of lower Jurassic gas reservoir of Northern Foothill Belt, Turpan-Hami Basin. Journal of Central South University (Science and Technology), 2012,43(1): 258-264 (in Chinese).
Liu, B., Huang, Z., Tu, X., Zhang, J., Mu, K., 2011. Structural styles and hydrocarbon accumulation of the northern piedmont belt in the Taibei Sag, Turpan-Hami Basin. Petrol. Explor. Dev. 38 (2), 152–158. https://doi.org/10.1016/S1876-3804(11)60023-2.
Liu, N., Qiu, N., Cai, C., Li, Z., Wang, Y., Jiao, Y., Gao, T., Sun, H., Lu, M., 2022. Geochemical characteristics and natural gas-oil-source correlation of the Shulu depression in the Jizhong Subbasin, Bohai Bay Basin, eastern China. J. Pet. Sci. Eng. 216, 110831 https://doi.org/10.1016/j.petrol.2022.110831.
Mackenzie, A., Leythaeuser, D., Muller, P., Quigley, T., Radke, M., 1988. The movement of hydrocarbons in shales. Nature 1988 331:6151, 331(6151), 63–65. Doi: 10.1038/331063a0.
Madec, M., Espitalié, J., 1985. Determination of organic sulphur in sedimentary rocks by pyrolysis. J. Anal. Appl. Pyrol. 8 (C), 201–219. https://doi.org/10.1016/0165-2370(85)80027-9.
Mann, A., Goodwin, N., Lowe, S., 1987. Geochemical characteristics of lacustrine source rocks: a combined palynological/molecular study of a tertiary sequence from offshore China. Indonesian Petroleum Association. 241–258. http://archives.datapages.com/data/ipa/data/016/016001/241_ipa016a0241.htm.
Mann, U., Hantschel, T., Schaefer, R., Krooss, B., Leythaeuser, D., Littke, R., Sachsenhofer, R., 1997. Petroleum migration: mechanisms, pathways, efficiencies and numerical simulations. Petroleum and Basin Evolution 403–520. https://doi.org/10.1007/978-3-642-60423-2_8.
Moldowan, J.M., 1984. C30-steranes, novel markers for marine petroleums and sedimentary rocks. GeochimicaEt Cosmochimica Acta 48 (12), 2767–2768. https://doi.org/10.1016/0016-7037(84)90321-1.
Moldowan, J., Seifert, W., Gallegos, E., 1985. Relationship between petroleum composition and depositional environment of petroleum source rocks. Am. Assoc. Pet. Geol. Bull. 69 (8), 1255–1268. https://doi.org/10.1306/AD462BC8-16F7-11D7-8645000102C1865D.
Ni, Y., Liao, F., Gong, D., Jiao, L., Gao, J., Yao, L., 2019. Stable carbon and hydrogen isotopic characteristics of natural gas from Taibei sag, Turpan-Hami Basin, NW China. Petrol. Explor. Dev. 46 (3), 531–542. https://doi.org/10.1016/S1876-3804(19)60033-9.
Pan, Y., Huang, Z., Li, T., Guo, X., Xu, X., Chen, X., 2020. Environmental response to volcanic activity and its effect on organic matter enrichment in the Permian Lucaogou Formation of the Malang Sag, Santanghu Basin, Northwest China. Palaeogeogr. Palaeoclimatol. Palaeoecol. 560, 110024 https://doi.org/10.1016/J.PALAEO.2020.110024.
Pang, B., Pang, X., Luo, B., Zheng, D., Xu, Z., Zhang, S., Chen, J., 2023. Influence of the Emeishan basalt eruption on hydrocarbon generation and expulsion characteristics of Sinian (Ediacaran) algal dolomite in Sichuan Basin. Journal of Analytical and Applied Pyrolysis, 169(December 2022), 105836. Doi: 10.1016/j.jaap.2022.105836.
Pang, X., Li, M., Li, S., Jin, Z., 2005. Geochemistry of petroleum systems in the Niuzhuang South Slope of Bohai Bay Basin: Part 3. Estimating hydrocarbon expulsion from the Shahejie formation. Org. Geochem. 36 (4), 497–510. https://doi.org/10.1016/J.ORGGEOCHEM.2004.12.001.
Pepper, A., 1991. Estimating the petroleum expulsion behaviour of source rocks: a novel quantitative approach. Geochem. Soc. Spec. Publ. 59, 9–31. https://doi.org/10.1144/GSL.SP.1991.059.01.02.
Pepper, A., Corvi, P., 1995. Simple kinetic models of petroleum formation. Part I: oil and gas generation from kerogen. Mar. Pet. Geol. 12 (3), 291–319. https://doi.org/10.1016/0264-8172(95)98381-E.
Peters, K.E., Cassa, M., 1994. Applied Source Rock Geochemistry. The Petroleum System—From Source to Trap, 93–120. Doi: 10.1306/M60585C5.
Peters, K., Moldowan, J., 1993. The biomarker guide: Interpreting molecular fossils in petroleum and ancient sediments. Prentice Hall, Englewood Cliffs, NJ (United States).
Peters, K.E., Walters, C.C., Moldowan, J.M., 2005. The Biomarker Guide. Biomarkers and Isotopes in Petroleum Exploration and Earth History. Cambridge University Press, New York.
Philp, R., Gilbert, T., 1986. Biomarker distributions in Australian oils predominantly derived from terrigenous source material. Org Geochem. 10 (1–3), 73–84. https://doi.org/10.1016/0146-6380(86)90010-0.
Powell, T., McKirdy, D., 1973. Relationship between Ratio of Pristane to Phytane, Crude Oil Composition and Geological Environment in Australia. Nature Physical Science 1973 243:124, 243(124), 37–39. Doi: 10.1038/physci243037a0.
Prinzhofer, A., Battani, A., 2003. Gas isotopes tracing: an important tool for hydrocarbons exploration. Oil Gas Sci. Technol. 58 (2), 299–311.
Ritter, U., 2003. Solubility of petroleum compounds in kerogen: Implications for petroleum expulsion. Org Geochem. 34 (3), 319–326. https://doi.org/10.1016/S0146-6380(02)00245-0.
Rohling, E., 2000. Paleosalinity: confidence limits and future applications. Mar. Geol. 163, 1–11.
Shen, J., Zhou, L., Feng, Q., Zhang, M., Lei, Y., Zhang, N., Yu, J., Gu, S.Z., 2014. Paleoproductivity evolution across the Permian-Triassic boundary and quantitative calculation of primary productivity of black rock series from the Dalong Formation, South China. Sci. China Earth Sci. 57, 1583–1594.
Shen, J., Schoepfer, S., Feng, Q., Zhou, L., Yu, J., Song, H., Wei, H., Algeo, T., 2015. Marine productivity changes during the end-Permian crisis and Early Triassic recovery. Earth Sci. Rev. 149, 136–162.
Sinninghe Damsté, J., Kenig, F., Koopmans, M., Köster, J., Schouten, S., Hayes, J., De Leeuw, J., 1995. Evidence for gammacerane as an indicator of water column stratification. Geochim. Cosmochim. Acta 59 (9), 1895–1900. https://doi.org/10.1016/0016-7037(95)00073-9.
Stoakes, F., Creaney, S., 1984. Sedimentology of a carbonate source rock: Duvernay formation of central Alberta. In: Eliuk, L. (Ed.), Carbonates in Subsurface and Outcrop, Proceedings of the 1984 Canadian Society of Petroleum Geologists Core Conference, pp. 132–147.
Stoakes, F., 1980. Nature and control of shale basin fill and its effect on reef growth and termination: upper devonian duvernay and ireton formations of alberta, canada f. a. 28(3), 345–410.
Sun, J., Xiao, X., Cheng, P., Wang, M., Tian, H., 2021. The relationship between oil generation, expulsion and retention of lacustrine shales: Based on pyrolysis simulation experiments. J. Pet. Sci. Eng. 196 https://doi.org/10.1016/j.petrol.2020.107625.
Sun, X., Zhang, T., Sun, Y., Milliken, K.L., Sun, D., 2016. Geochemical evidence of organic matter source input and depositional environments in the lower and upper Eagle Ford Formation, south Texas. Org Geochem. 98, 66–81. https://doi.org/10.1016/J.ORGGEOCHEM.2016.05.018.
Taylor, S., McLennan, S., 1985. The Continental Crust: its Composition and Evolution. Blackwell Scientific Publications, Oxford.
Ten Haven, H., de Leeuw, J., Rullkötter, J., Damsté, J., 1987. Restricted utility of the pristane/phytane ratio as a palaeoenvironmental indicator. Nature 1987 330:6149, 330(6149), 641–643. Doi: 10.1038/330641.
Tissot, B., Welte, D., 1984. Petroleum formation and occurrence. Springer-Verlag. https://doi.org/10.1007/978-3-642-87813-8.
Wang, E., Liu, G., Pang, X., Li, C., Zhao, Z., Feng, Y., Wu, Z., 2020. An improved hydrocarbon generation potential method for quantifying hydrocarbon generation and expulsion characteristics with application example of Paleogene Shahejie Formation, Nanpu Sag, Bohai Bay Basin. Mar. Pet. Geol. 112, 104106 https://doi.org/10.1016/J.MARPETGEO.2019.104106.
Wang, E., Guo, T., Li, M., Xiong, L., Dong, X., Zhang, N., Wang, T., 2022a. Depositional environment variation and organic matter accumulation mechanism of marine-continental transitional shale in the upper permian Longtan Formation, Sichuan Basin, SW China. ACS Earth Space Chem. 6 (9), 2199–2214. https://doi.org/10.1021/acsearthspacechem.2c00101.
Wang, E., Li, C., Feng, Y., Song, Y., Guo, T., Li, M., Chen, Z., 2022b. Novel method for determining the oil moveable threshold and an innovative model for evaluating the oil content in shales. Energy 239 (A), 121848.
Wei, W., Algeo, T., 2020. Elemental proxies for paleosalinity analysis of ancient shales and mudrocks. GeochimicaEt Cosmochimica Acta 287, 341–366. https://doi.org/10.1016/j.gca.2019.06.034.
Wilhelms, A., Larter, S., Leythaeuser, D., Dypvik, H., 1990. Recognition and quantification of the effects of primary migration in a Jurassic clastic source-rock from the Norwegian continental shelf. Org Geochem. 16 (1–3), 103–113. https://doi.org/10.1016/0146-6380(90)90030-4.
Wu, Z., Zhao, X., Pu, X., Wang, E., Dong, X., Li, C., 2022. Petroleum resource potential evaluation using insights based on hydrocarbon generation, expulsion, and retention capabilities—a case study targeting the Paleogene Es1 formation, Qikou Sag. J. Pet. Sci. Eng. 208 https://doi.org/10.1016/j.petrol.2021.109667.
Zhang, S., Liu, C., Liang, H., Wang, J., Bai, J., Yang, M., Liu, G., Huang, H., Guan, Y., 2018. Paleoenvironmental conditions, organic matter accumulation, and unconventional hydrocarbon potential for the Permian Lucaogou Formation organicrich rocks in Santanghu Basin, NW China. Int. J. Coal Geol. 185, 44–60.
Zheng, R., Zeng, W., Li, Z., Chen, X., Man, K., Zhang, Z., Wang, G., Shi, S., 2022. Differential enrichment mechanisms of organic matter in the Chang 7 Member mudstone and shale in Ordos Basin, China: constraints from organic geochemistry and element geochemistry. Palaeogeogr. Palaeoclimatol. Palaeoecol. 601 (June), 111126 https://doi.org/10.1016/j.palaeo.2022.111126.